SCALING EFFECTS OF 5- TO 13-kW TURBOELECTRIC UNMANNED AIRCRAFT POWER SYSTEMS

By

TIMOTHY RAYMOND RUNNELS

Bachelor of Science in Aerospace Engineering

Bachelor of Science in Mechanical Engineering

Oklahoma State University

Stillwater, Oklahoma

2020

Submitted to the Faculty of the
Graduate College of the
Oklahoma State University
in partial fulfillment of
the requirements for
the Degree of
MASTER OF SCIENCE
May, 2022

SCALING EFFECTS OF 5- TO 13-kW

TURBOELECTRIC UNMANNED

AIRCRAFT POWER SYSTEMS

Thesis Approved:

Kurt Rouser

Thesis Adviser

Jamey Jacob

Richard Gaeta

Name: TIMOTHY RAYMOND RUNNELS

Date of Degree: MAY, 2022

Title of Study: SCALING EFFECTS OF 5- TO 13-kW TURBOELECTRIC UNMANNED AIRCRAFT POWER SYSTEMS

Major Field: MECHANICAL AND AEROSPACE ENGINEERING

Abstract:

This thesis details ground tests of three different turboelectric systems for unmanned aircraft applications based on existing 5-kW, 7-kW and 13-kW turbine engines. The motivation for this study is the continuing emergence of hybrid gas-electric power systems for manned and unmanned aircraft to extend the range over battery-only aircraft and decrease carbon emissions associated with hydrocarbon fuels. However, there is currently a lack of published experimental performance data on turboelectric power systems, though there are many paper designs and analytical studies of aircraft turboelectric systems. This thesis compares the effect of scale in performance parameters by comparing the three different turboelectric systems. A bench test stand with representative electrical loads was built and used for static ground testing of these turboelectric systems. Steady-state tests measured turboelectric system fuel usage and power production for calculating brake specific fuel consumption and power-to-weight ratio of the turboelectric systems. Transient tests measured response time and rate-of-change of power. Data from both steady state and transient tests highlight electrical safety challenges. A better understanding of the effects of scale on turboelectric system will allow for better performance estimates for design purposes, inform mission planning for unmanned aircraft, and enable future comparisons of turboelectric systems to piston-based hybrid gas-electric systems and battery-only systems for unmanned aircraft.

TABLE OF CONTENTS

Chapter Page

INTRODUCTION 1
Motivation 1
Solution 4
Objectives 5
Background 7
Previous Works 7
Theory 13
Design 13
Turbine engine/turboprop background 15
Turbine Engine Parametric Cycle Analysis 18
Electric Motors and Generators 22
Control methodologies for the gas turbine engine 24
Methodology 28
Experimental Setup 28
Turboelectric System 28
Test Bench 31
Procedure 33
Steady State 33
Transient 34
Parametric Cycle Analysis Predictions 35
K-45TP 36
K-60TP 37
K-100TP 38
Comparison to other electrified propulsion 38
Results 40

Chapter Page

Steady State Performance 40
DTC Performance 40
Uncertainty 46
ATC Performance 47
Transient Performance 53
Identification of transient endpoints 53
DTC Performance 55
DTC Performance Discussion 61
ATC Performance 62
ATC Performance Discussion 69
Electrical Safety 70
Summary and Conclusions 76
Steady State 76
Transient 77
Electrical Safety 78
Conclusion 79
REFERENCES 80
APPENDICES 84
Parametric Cycle Analysis 84
VITA 1

LIST OF TABLES

Table Page

Table 1.Turboelectric system mass 31
Table 2. Test Equipment 33
Table 3. Fluid properties for PCA 36
Table 4. K-45TP PCA inputs 36
Table 5. K-45TP PCA results 37
Table 6. K-60TP PCA inputs 37
Table 7. K-60TP PCA results 37
Table 8. K-100TP PCA inputs 38
Table 9. K-100TP PCA results 38
Table 10. Performance of the Harris Aerial H5000 generator 39
Table 11. Summary of DTC 5-kW Turboelectric performance at different throttle settings 45
Table 12. Summary of DTC 7-kW Turboelectric performance at different throttle settings 45
Table 13. Summary of DTC 13-kW Turboelectric performance at different throttle settings 45
Table 14. Maximum power-to-weight ratio of each DTC turboelectric system. 46
Table 15. Summary of ATC 5-kW Turboelectric performance at different throttle settings 52
Table 16. Summary of ATC 7-kW Turboelectric performance at different throttle settings 52
Table 17. Summary of ATC 13-kW Turboelectric performance at different throttle settings 52
Table 18. Maximum power-to-weight ratio of each ATC turboelectric system. 53
Table 19. DTC 5-kW positive step change in throttle position power data 56
Table 20. DTC 5-kW negative step change in throttle position power data 57
Table 21. DTC 7-kW positive step change in throttle position power data 58
Table 22. DTC 7-kW negative step change in throttle position power data 59
Table 23. DTC 13-kW positive step change in throttle position power data 60
Table 24. DTC 13-kW negative step change in throttle position power data 61
Table 25. DTC Positive-step response time and average slope results 62
Table 26. DTC Negative-step response time and average slope results 62
Table 27. ATC 5-kW positive step change in throttle position power data 64
Table 28. ATC 5-kW negative step change in throttle position power data 65
Table 29. ATC 7-kW positive step change in throttle position power data 66
Table 30. ATC 7-kW negative step change in throttle position power data 67

Table Page

Table 31. ATC 13-kW positive step change in throttle position power data 68
Table 32. ATC 13-kW negative step change in throttle position power data 69
Table 33. ATC positive-step response time and average slope results 70
Table 34. ATC negative-step response time and average slope results 70
Table 35. Maximum current during the steady state tests 71
Table 36. Ending voltage of 100%-50% transient tests 75

LIST OF FIGURES

Figure Page

Figure 1. A basic Schematic of a Turboelectric system 1
Figure 2. A Photo of the 13-kW system 5
Figure 3. NASA turboelectric commercial transport concept aircraft [6] 8
Figure 4. An image of several NASA UAM concepts [15] 10
Figure 5. Notional diagram of partial and fully turboelectric systems [45] 13
Figure 6. Notional diagram of a partial turboelectric system with a battery in parallel [45] 14
Figure 7. A photo of the Kingtech K-100TP secondary turbine. Additionally, the exhaust manifold can be seen behind the turbine 16
Figure 8. A diagram showing the main components of a separate-shaft small turboprop engine . 17
Figure 9. A diagram showing the main components of a concentric-shaft turboprop engine 17
Figure 10. A photo of the 13-kW turboelectric system showing key components 22
Figure 11. A schematic of the DTC operating mode 25
Figure 12. A schematic of the ATC operating mode 25
Figure 13. A basic control block diagram of the ATC controller. 27
Figure 14. A photo of a Kingtech K-45TP 29
Figure 15. Left: the 5-kW turboelectric system, Right: the 7-kW turboelectric system, Center: the 13-kW turboelectric system 29
Figure 16 A photo of the bench test stand with the K-60TP-based system installed, showing the available electric loads of the 28 in. propeller motor and two additional five kW EDFs. 32
Figure 17. A photo of the Mauch power module used to measure voltage and current between the turboelectric system and the load. (Both lines were used during testing) 33
Figure 18. An example of current (left) and voltage (right) acquired from the Pixhawk during the 100% throttle test of the DTC 13-kW system 41
Figure 19. Trend in power output for the DTC turboelectric systems with linear fits 42
Figure 20. Trend in BSFC data for the DTC turboelectric systems with a third order polynomial fit 44
Figure 21. K-45 ATC Voltage Drop. (left) The voltage of the ATC 5-kW system at 100% throttle showing a voltage decrease as the battery depletes. (Right) The voltage of the ATC 5-kW system at 25% throttle showing no notable voltage drop. 48
Figure 22. Data from the BMS showing current and voltage from the ATC 5-kW 100% throttle test 48
Figure 23. Data from the BMS showing current and voltage from the ATC 5-kW 25% throttle test 49
Figure 24. Trend in power output for the DTC turboelectric systems with linear fits 50

Figure Page

Figure 25. Trend in BSFC data for the DTC turboelectric systems 51
Figure 26. An example of transient throttle data displaying current as a function of time. The endpoints of the transient are marked in red. 54
Figure 27. A plot showing measured currents, a running average, and positive multiples of the standard deviation 54
Figure 28. DTC 5-kW positive step changes in throttle position with endpoints marked 56
Figure 29. DTC 5-kW negative step changes in throttle position 57
Figure 30. DTC 7-kW positive step changes in throttle position 58
Figure 31. DTC 7-kW negative step changes in throttle position 59
Figure 32. DTC 13-kW positive step changes in throttle position 60
Figure 33. DTC 13-kW negative step changes in throttle position 61
Figure 34. ATC 5-kW positive step changes in throttle position 63
Figure 35. ATC 5-kW negative step changes in throttle position 64
Figure 36. ATC 7-kW positive step changes in throttle position 66
Figure 37. ATC 7-kW negative step changes in throttle position 67
Figure 38. ATC 13-kW positive step changes in throttle position 68
Figure 39. ATC 13-kW negative step changes in throttle position 69
Figure 40. A plot of voltage over time for the ATC 5-kW negative step transient tests 72
Figure 41. A plot of voltage over time for the ATC 7-kW negative step transient tests 73
Figure 42. A plot of voltage over time for the ATC 13-kW negative step transient tests 73
Figure 43. A plot of voltage over time for the DTC 13-kW negative step transient tests 74

CHAPTER I

INTRODUCTION

Motivation

Emerging gas-electric hybrid aircraft utilizing gas turbine engines have many technical challenges that require real world test data and practical knowledge, rather than purely theoretical and analytical design studies. These turbine-based gas-electric hybrid power systems are known as turboelectric power systems. Turboelectric systems present potential benefits over piston-based hybrid electric systems such better performance at high altitudes, lower vibrational loads, and a greater variety of fuels that can be used. A basic schematic of a turboelectric system can be seen in Figure 1 which highlights the key components of the system. The key components include a turbine engine, a generator, and a rectifier. There have been many theoretical studies performed for turboelectric systems, but there is a dearth of real-world tests on these systems. Many questions remain over the performance and safety challenges of turboelectric systems in aircraft. The performance and integration of turboelectric systems is going to be a key area of study as new designs for commercial aircraft, urban air mobility (UAM) aircraft, and unmanned aircraft are being investigated.

Figure 1. A basic Schematic of a Turboelectric system

Commercial aircraft, UAM aircraft and unmanned aerial vehicles (UAV's) have significant different power and integration requirements. UAV's typically have powerplants producing less than 100-kW of power. UAM aircraft have power requirements between 150-kW and 1-MW. Commercial aircraft typically have power requirements above 1-MW. Therefore, these different scales of systems come with unique challenges and characteristics. The difficulties of designing aircraft to utilize turboelectric systems is exacerbated by the limited real-word test data on these systems. Thus, there is a critical need to improve understanding of how the size of turboelectric systems affects performance and electrical safety of the system for integration into turboelectric aircraft. A better understanding of the effects of scale on turboelectric performance can help influence future designs of hybrid electric systems.

To address this critical need, turboelectric systems could be fabricated and tested at each of the different scales discussed above. It is impractical to test across these different size ranges. Each system would need an independent test setup. (i.e. there would need to be entirely different measurement devices for the large megawatt-class commercial aircraft turboelectric systems and kilowatt-class UAV turboelectric systems.)

Unmanned aircraft-scale turboelectric systems with less than 20-kW output provide the least risk to schedule, cost, and safety. Larger turbine engines are more expensive and require longer lead times for purchases, repairs, and installation than unmanned aircraft-scale turbine engines. General aviation and commercial turbine engines also require highly trained personnel for maintenance and operation. Unmanned aircraft turbine engines are cheaper and can be operated by personnel who are not pilots or aircraft mechanics. The measurement equipment for these systems is cheaper than that of larger turbine engines, and there is less needed in terms of ground support equipment.

The effects of scale on UAV turboelectric systems are not experimentally validated. The overall efficiency of a hybrid propulsion system is the product of the thermal efficiency of the system,

the propulsive efficiency of the system, and the electrical efficiency of the system. The thermal efficiency of a turbine engine is inversely proportional to the compressor pressure ratio, meaning that the engine gets more efficient with a higher compressor pressure ratio. The small scale of UAV turbine engines limits the compressor performance due to the geometric constraints of UAV turbine engines. Therefore, at the UAV scale, Compressor Pressure Ratio (CPR) increases as turbine engine scale increases, and consequently thermal efficiency also increases.

The propulsive efficiency of the propulsion system depends primarily on the configuration of the aircraft the system is installed into. For a fixed thrust, a higher mass flow rate of the propulsor working fluid will lead to a lower acceleration of the working fluid. The lower acceleration of the working fluid leads to an increase in propulsive efficiency. The increased mass flow rate can be achieved with a hybrid system by distributing multiple smaller propulsors around the aircraft or including one larger propulsor. In either case, as system scale increases, so does the overall power demand (even if the efficiency is increasing). As the DC power transmitted through a system increases, if voltage is constant, the current sent through the system will increase. With constant system voltage, electrical efficiency is inversely proportional to current. Consequently, at a constant voltage, the electrical efficiency decreases as system scale increases. In a ground test configuration, only electrical and thermal efficiency can be studied. Propulsive efficiency is undefined when the propulsion system is stationary. It is possible to study how thermal and electrical efficiency scale independent of the propulsive efficiency by modeling the power demand of the propulsors with simulated loads.

It is not readily apparent which effect dominates between increasing thermal efficiency and decreasing electrical efficiency with increasing scale, and whether the overall efficiency of UAV turboelectric systems increases or decreases as system scale increases. It is also not known whether the scale of turboelectric system impacts the dynamic response of the system. The size of a gas turbine engine has an impact on the inertia of the turbomachinery and generator, which

could impact the response of the electrical system. It is also not known how the inclusion of a battery could impact the dynamic response of the system. As scale increases, current and power transmitted through the electrical system increases, so it is important to investigate how the increased power of larger systems impacts electrical safety in steady performance. The scale of system may also impact the safety of the system during dynamic tests, especially as more power can lead to larger deviations in voltage and current during transient loading.

This paper seeks to answer the question, "What is the effect of turboelectric power system scale on power production, dynamic response, and electrical safety?"

Solution

Ground tests can be used to measure the performance of turboelectric systems. Ground testing allows for more precise control of the power output and demand than flight testing can offer. In flight testing, the power demand is driven by the operation of the aircraft and must constantly be adjusted to keep the aircraft airborne. Ground tests also allow for difficulties in the system design to be worked out before taking on the risk of flying an aircraft. A combination of steady state and transient testing can illuminate the steady state performance, dynamic response, and the electrical safety issues of these turboelectric systems.

Three different UAV turboelectric power systems were designed and constructed, based off Kingtech turboprop engines. The smallest turboelectric system built was based on a Kingtech K-45TP, which has a rated power output of 5.2-kW. The middle-sized turboelectric system was based on a Kingtech K-60TP with a rated power output of 7.3-kW. The largest of these turboelectric systems was based on a Kingtech K-100TP with a rated power output of 13.0-kW. Henceforth these systems will be referred to by their turboprop's rated shaft-power output. All three systems are relatively similar in design, though there are differences in housing designs and generator choices between all three systems. The K-100TP based system can be seen in Figure 2.

These systems were tested and compared to determine the impact of scale between the three systems.

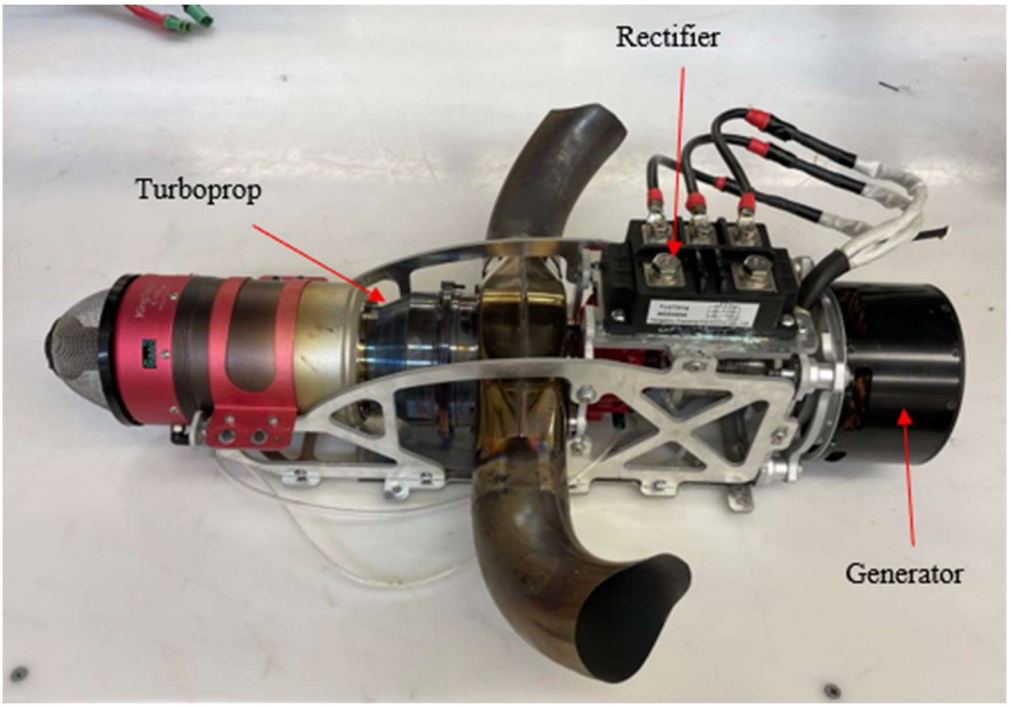

Figure 2. A Photo of the 13-kW system

Objectives

The objectives of this study are:

1) Compare steady-state performance of three different UAV turboelectric systems based on turbine engines rated for 5-kW, 7-kW and 13-kW shaft power output over a range of throttle settings. Steady-state figures of merit include Maximum power output, power to weight ratio, and brake specific fuel consumption (BSFC).
2) Compare transient response of the three engines to different throttle inputs. The primary transient figures of merit are response time and the slope of the power vs. time curve.

3) Assess electrical safety issues, such as peak voltage and current reached by the three different turboelectric systems.

The three turboelectric systems were run through ground tests with and without battery. These tests included both steady state and transient ground tests to assess safety and performance. The steady state performance of these UAV turboelectric systems can be benchmarked against commercially available piston-hybrid UAV hybrid-electric systems such as the Herris Aerial H5000 Generator [1].

CHAPTER II

Background

Previous Works

Previous work with turboelectric aircraft systems have addressed challenges in the design and construction of turboelectric power systems. At the largest scales (>1MW), turboelectric power systems are being studied to reduce the emissions of commercial aircraft. There is concern for the impact of aviation on the global climate. Commercial air travel accounts for 2-3% of humanities' CO_2 output every year [2]. Multiple authors have studied methods to decrease fuel usage by using new technologies with traditional turbofan engines, such as turbofan gearboxes, or by utilizing a triple spool design [3–5]. While these show promise to reduce fuel consumption, they do not cover any electrification of commercial aircraft. The National Aeronautics and Space Administration (NASA) has been investigating methods to reduce the usage of aviation fuel by commercial aircraft with electrified propulsion. Their current turboelectric concepts include the ECO-150 with Empirical Systems Aerospace, the Subsonic Ultra Green Aircraft Research (SUGAR) with Boeing, the N3-X and STARC-ABL concepts shown in Figure 3[6] .

Figure 3. NASA turboelectric commercial transport concept aircraft [6]

Westlead and Felder investigated a design for a single-aisle commercial aircraft (STARC-ABL in Figure 3) [7]. This aircraft design is propelled an arrangement of two turbofan engines mounted under-wing with a boundary layer ingesting electric fan in the rear. The STARC-ABL would power its electric fan with electrical power pulled from the turbofan engines, while still using thrust from the turbofan engines. Multiple authors at NASA have investigated the use of turboelectric systems to reduce the usage of aviation fuel in a hybrid-wing-body commercial aircraft (N3-X in Figure 3) [8–10]. The N3-X design is fully turboelectric, where all the power generated by the turbine engines of the aircraft is transformed into electrical power and used to drive electric fans distributed along the body of the aircraft. The N3-X design reduces fuel usage with a low drag lifting-body airframe design, distributed electric propulsion, and boundary layer ingestion. Empirical Systems Aerospace has been working with NASA to design a turboelectric tube-and-wing aircraft (the ECO-150 shown in Figure 3)[11,12]. The ECO-150 utilizes distributed propulsion like the N3-X but does not include boundary layer ingestion with the distributed electric fans. The ECO-150 design is a tube-and-wing, unlike the N3-X design, allowing for easier integration into existing airport architecture. All of the above designs NASA has researched show potential to reduce emissions of commercial aircraft but are all at a large scale (>1-MW) and are lacking in real-word test data. Pornet et al. created a methodology to size the hybrid powertrain components of a turboelectric aircraft, including the turbine engine,

batteries, and propulsors for the aircraft [13]. Mission analysis showed a reduction of 16% fuel use compared to a reference airliner by using the hybrid optimization scheme proposed. While Pornet et al. discussed how to properly size turboelectric systems for commercial airliners, it does not have empirical validation of the optimization model proposed.

NASA has been investigating the use of UAM aircraft as a method to avoid congestion in ground-based transport. UAM aircraft can utilize turboelectric systems between 100-kW to 1-MW. Thipphavong et al. discussed how UAM has existed since the 1960's in the form of helicopter airlines. With technological advances such as autonomy, composite structures and electrification and potential economic opportunities, the use of UAM aircraft is expected to increase, and NASA is investigating methods to integrate these aircraft into our airspace and cities [14]. Some examples of NASA concept UAM vehicles can be seen in Hendricks et al. Hendricks et al. investigated how to optimize a UAM aircraft between multiple criteria such as engine, rotor, and airframe [15][15]. Hendricks et al. presented the optimization of a tilt-wing turboelectric UAM as an example, and discussed how optimizing one system (i.e. optimizing for the internal combustion engine only) will not perform as well as an optimization between multiple design criteria (structural, propulsion, controls, ect.). As discussed previously, UAM aircraft have power requirements between 100-kW and 1-MW, so the systems studied with UAM aircraft are at a larger scale than those considered in this paper. Some larger unmanned aircraft have power requirements near the range of UAM aircraft. Cinar et al. and Markov et al. investigated a turboelectric retrofit to reduce the fuel usage of a military UAV with a power requirement of 750-kW [16,17]. Results showed a 10-30% reduction in fuel use over a simulated mission. Like other turboelectric research in this power range, the results are based on a simulated mission, and do not include empirical results.

Figure 4. An image of several NASA UAM concepts [15]

There is also interest in turboelectric systems that produce less than 20-kW for unmanned aircraft. Some of the earliest works in hybrid-electric propulsion investigated the use of piston engines alongside solar-electric propulsion[18]. Harmon et al. investigated the use of a piston hybrid-electric propulsion in unmanned aircraft[19]. Simulation results showed increase range and loiter time compared to fully-electric aircraft and decreased noise and thermal signature compared to piston-driven aircraft. While this paper did cover a hybrid-electric unmanned aircraft, the hybrid system was based on a piston engine, not a turbine engine. Multiple authors have looked at control methodologies for piston-based hybrid-electric systems [20–23], but there is a lack in literature studying modeling and control aspects of turbine-based hybrid systems for unmanned aircraft. There are multiple studies that have investigated modelling and control for commercial aircraft, but these typically involve multiple turbine engines and turboelectric systems based off turbofan engines unlike smaller unmanned aircraft turboelectric systems [24–26]. Zong et al. compared turboelectric hybrid, piston-hybrid, and fully electric arrangements for a Vertical takeoff and landing (VTOL) UAV [27]. Zong et al found that the fully electric variant of the aircraft had the highest required propulsion weight, with turboelectric being the second heaviest, and piston-hybrid being the lightest. Similar to most studies discussed thus far, the comparison between these systems is based entirely on simulation. Eqbal et al. proposed a design for an unmanned aircraft turboelectric system using a Kingtech K-45TP [28]. The design presented by Eqbal et al. replaced the starter motor of the K-45TP with a starter-generator with an intended

power output of 2-kW. Results showed that the turboelectric design has the potential of reducing the weight of the K-45 TP by 30% by removing the secondary turbine and gearbox of the turboprop. Eqbal et al. also investigated the use of distributed electric propulsion on a UAV with this turboelectric system. Results showed with the reduced weight of the turboelectric system and benefits from increased propulsive efficiency from distributed propulsion, the aircraft could be capable of up to a 98% increase in range compared to the same aircraft in a turboprop configuration. This paper did not provide any test validation of the power output or range benefits for the unmanned aircraft. Other research work has focused directly on the design of turboelectric power systems rather than their integration into UAV airframes.

Badum et al. investigated the conceptual design of a small turboelectric system with a design power output of 300-W [29]. Badum et al. sought to overcome the issues other small turboelectric designs have encountered by using dental tool bearings to handle the high shaft speed of a 300-W turbine engine. The turbogenerator was designed with the compressor and turbine built onto a monolithic shaft with a cantilever section to ensure heat from combustion did not damage the dental bearings. Badum et al. highlighted that further advancements in metallic additive manufacturing would need to be made to construct this turboelectric system with the necessary precision to reach their performance goals. There has been significant interest in the creation of turboelectric systems in the 10-W to 100-W range, with multiple authors across different organizations attempting to study engines in this size range [30–34]. A few examples of these <100-W turbine engines were built and tested. So far none have been successful in producing a measurable electrical power output.

The Korean institute of Machinery and Materials (KIMM) has developed a design and simulation of a 500-W turboelectric system.[35]. The simulation work done in this study helped set the design choices for the turbine, including a compression ratio of 3.0, a shaft speed of 400,000-RPM, and a mass-flow rate of 20g/s. After further work designing and testing components,

KIMM was able to achieve a sustained 2-minute test on their turbogenerator [36,37]. The initial test performed on the turbine engine did not include a generator on the shaft, rather the test was performed to prove that the turbine engine was capable of sustained operation. KIMM continued work on the turbogenerator and added a generator to the turbine engine [38]T. Experiments showed that the turbogenerator was capable of generating 5-W of electrical power when operating at 35% of its design shaft speed under normal operational mode. The system was capable of generating up to 30-kW when operating at 50% of its shaft speed while using the starter fuel as a main fuel source in the turbogenerator's "boosted" operating mode. The work at KIMM provides information on the experimental performance of a clean sheet design of a turboelectric system. Their work however has not yet covered the experimental performance of turboelectric systems at different sizes or performance when operating at a turbine engine's maximum throttle setting.

Previous works at Oklahoma State University have investigated the use of turboelectric systems for unmanned aircraft. Rouser et al. designed a turboelectric system using a Kingtech K-60TP and performed a representative power generation experiment using an electric motor to represent the power provided by the K-60TP [39]. Results showed electrical efficiencies up to 63% and validated the electrical system model developed for the turboelectric system. While this paper presented experimental results for the electrical side of a turboelectric system, it did not involve tests with a turbine engine. Moody et al. developed an electrical system model for the turboelectric system designed by Rouser et al. [40–42]. Results showed electrical efficiencies up to 77% and that predicted voltage values were close to experimental voltage values. Like Rouser et al, Moody et al. used an electric motor to model the turboprop engine in experiments and did not show experimentally how turbine performance effects overall system performance. Runnels et al. performed steady state experiments with the three turboelectric systems presented in this paper, but only presented results for the turbogenerator with no battery in parallel [43]. Burgess et

al investigated the transient response of the 7-kW turboelectric system[44]. Results showed that including a battery in parallel with the turbogenerator improved system response time. Burgess et al. only investigated the K-60TP based turboelectric system and did not compare response times between the different turboelectric systems.

Theory

Design

The core theory of turboelectric power systems integrates both turbine engines and electrical generation. As mentioned previously, the key elements of a turboelectric system are a gas turbine engine, designed either as a turboshaft or turboprop, and an electrical generator. Different configurations of turbine engine, generator, and battery are possible. In a fully turboelectric system, all power generated by a turbine is used to spin the generator. In a partially turboelectric system, some shaft power is used to generate electrical power, and some shaft power is used to operate a fan or propeller. Figure 5 shows a notional diagram of partial and fully turboelectric systems. A battery can be used in parallel with the turbogenerator. This is known as a parallel hybrid. A notional parallel hybrid configuration can be seen in Figure 6.

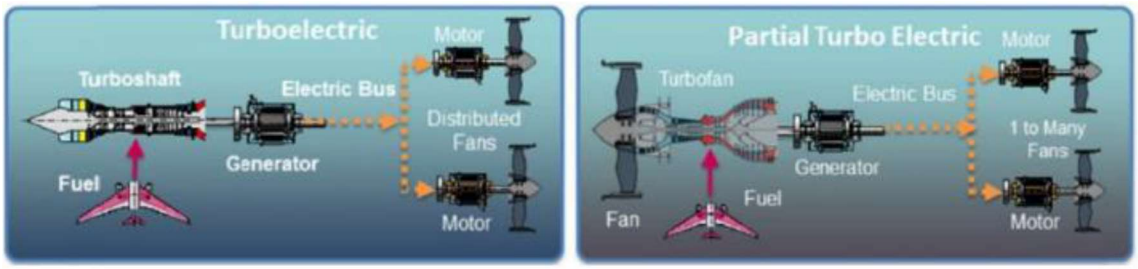

Figure 5. Notional diagram of partial and fully turboelectric systems [45]

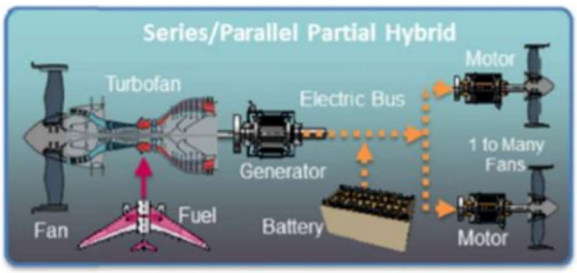

Figure 6. Notional diagram of a partial turboelectric system with a battery in parallel [45]

The turboelectric designed for this study were made from mostly commercial off the shelf (COTS) parts. A stock Kingtech turbine was coupled to a brushless direct current (DC) motor to be used as a generator in a fully turboelectric arrangement. The system was additionally designed to have a battery included for some tests with a parallel hybrid configuration. The generator produces 3-phase Alternating Current (AC) power. Most unmanned aircraft use DC power, so this AC power from the generator must be rectified to DC power. Rectification is done with a solid-state full-wave bridge rectifier. This DC power can be distributed between loads as required by the design of the test bench or aircraft.

The challenges faced by UAS hybrid propulsion and power systems include weight, complexity, and energy conversion/transmission efficiency. The increased weight and complexity of hybrid systems is due to the necessary inclusion of both electric and combustion components, whether in parallel or series configurations. Furthermore, low compression ratios inherent to small combustion engines result in poor thermal efficiency; however, overall efficiency and fuel economy can be preserved by increasing the propulsive efficiency with large or distributed propulsors. For example, multiple electric-driven fans, propellers, or rotors improve propulsive efficiency by accelerating a larger mass of air to a lower velocity compared to a single small-diameter fan, propeller, or rotor of equivalent thrust. In the context of a turbine engine, Equation 1 shows that ideal Brayton cycle thermal efficiency (η_{th}) is primarily a function of compressor pressure ratio (CPR), where "γ" is the ratio of specific heats, and propulsive efficiency (η_p) is a

function of propulsive fluid exit velocity (V_9). Thermal efficiency increases with CPR, and propulsive efficiency increases as V_9 decreases. Equation 3 shows that gas turbine engine overall efficiency is the product of thermal and propulsive efficiency. Thus, a small gas turbine engine constrained by geometry to low CPR and low thermal efficiency may still be viable with a high propulsive efficiency associated with a low acceleration of a propulsive fluid. The equation for overall hybrid gas-electric propulsion system efficiency (η_h), includes electric efficiency (η_e) associated with losses in electrical generation, conditioning, and transmission. Thus, even a small, turboelectric system can possibly achieve a higher propulsive efficiency with multiple electric-driven fans, propellers, or rotors, but the consequence of additional electric motors is even greater weight, complexity, and electrical system loss. This consequence presents a trade-off between performance and versatility, which is part of the motivation for this current study.

$$\eta_{th} = 1 - 1/[(CPR)^{(\gamma-1)/\gamma}] \quad (1)$$

$$\eta_p = 2/(1 + V_9/V_0) \quad (2)$$

$$\eta_O = \eta_{th} * \eta_p \quad (3)$$

$$\eta_h = \eta_{th} * \eta_p * \eta_e \quad (4)$$

Turbine engine/turboprop background

All 3 turboelectric systems use Kingtech turboprop engines. Kingtech turboprop engines are similar to larger turboprop engines. A gas generator (also known as the core) is used to generate hot, energetic gasses to spin a power output turbine. The core of the jet engine is formed by a compressor, combustor, and turbine. All kingtech turbines utilize a centrifugal compressor. Larger turboprop engines like the Allison T56 utilize a multi-stage axial compressor. While Kingtech does not publish compression ratios for their engines, they are estimated to have a compression ratio between 1.8 and 2.2. After the combustor, there is a single stage axial turbine which powers the compressor of the engine. Kingtech uses the same turbine core for their turbojet

and turboprop engines. Kingtech turbojet engines accelerate this flow through a nozzle to generate thrust. On the turboprop models, this flow is instead passed through a second, single-stage turbine to power the turboprop output shaft. A photo of the second stage turbine of the K-100TP can be seen in Figure 7.

Figure 7. A photo of the Kingtech K-100TP secondary turbine. Additionally, the exhaust manifold can be seen behind the turbine.

The second stage turbine has its power sent through a gear reduction box which steps down the RPM by a factor of 10. Gear reduction boxes are a common feature of turboprop engines, as this allows the propeller to operate at a lower RPM than the secondary turbine. The secondary turbine of the kingtech engines is entirely separate from the core of the turbine. Figure 8 shows a simplified depiction of a small turboprop engine, including shaft connections to illustrate how the

secondary turbine is entirely disjoint from the core turbine. This separated shaft design is different than some larger turbines where a concentric shaft is used to transfer power to the front of the engine where the gearbox and propeller are located. After the exhaust gas is used to power the secondary turbine, it is routed out of the engine through exhaust pipes.

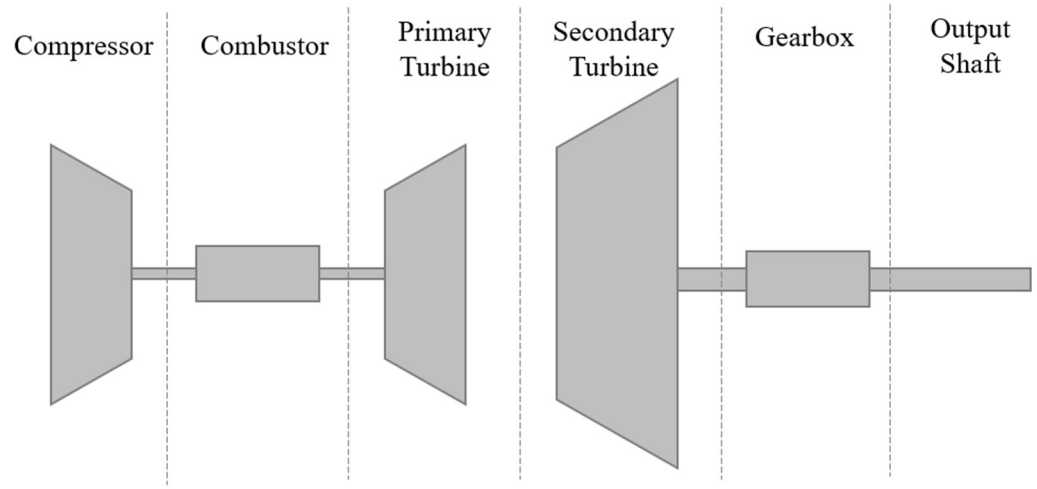

Figure 8. A diagram showing the main components of a separate-shaft small turboprop engine

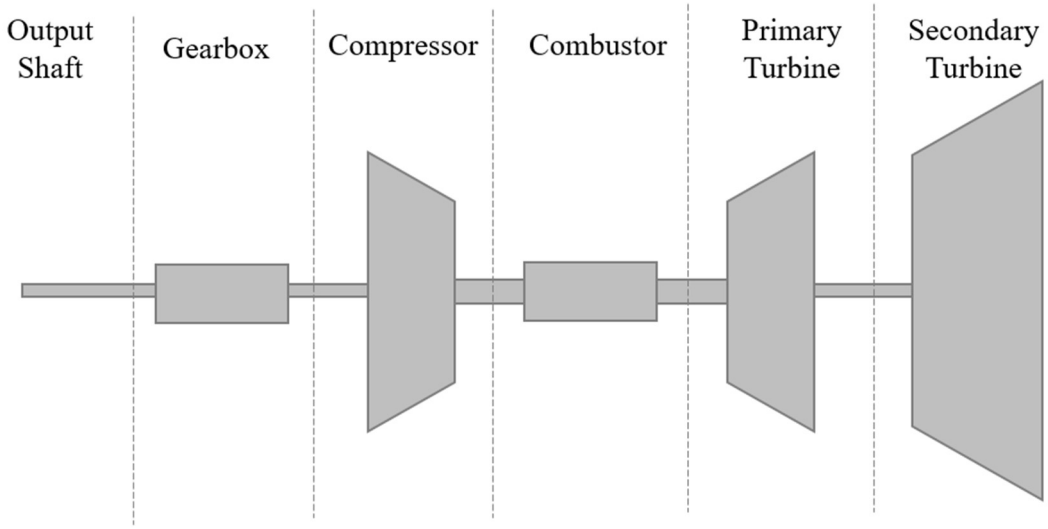

Figure 9. A diagram showing the main components of a concentric-shaft turboprop engine

Brake Specific Fuel Consumption (BSFC) is a figure of merit that can be used to compare the performance of different turboprop and turboshaft engines. As shown in equation 5, BSFC is a measure of how much fuel is used per unit power. Typically, the power term in equation 5is shaft power, though in this new area of study, the power in the denominator of equation 5 is DC electrical power delivered by the turboelectric system.

$$BSFC = {\dot{m}_{fuel}}/{P} \quad (5)$$

$\dot{m}_{fuel}$ is the mass flowrate of the fuel and P is the usable DC electrical power coming off the rectifier. $\dot{m}_{fuel}$ is a quantity which can be derived by weighing fuel throughout a test (the process for this is described below).

Another important figure of merit for aircraft power systems is the power to weight ratio (PWR). The power to weight ratio is defined as:

$$PWR = {P}/{W} \quad (6)$$

Weight is always an important consideration for aircraft power systems. The weight of an aircraft has a direct impact on the aircraft L/D ratio and climb performance. It is therefore desirable to have a high PWR because this means there is more power available at a lower weight.

Turbine Engine Parametric Cycle Analysis

Parametric cycle analysis (PCA) is a method is predicting turbine engine performance. The details of how to perform a parametric cycle analysis can be found in Elements of Propulsion by Mattingly and Boyer [46]. An overview of parametric cycle analysis will be presented here.

A PCA takes inputs of engine design limits, design choices, component performance, and fluid properties.

- Turbine inlet temperature: T_{T4}
- Compressor pressure ratio: π_c

- Burner pressure ratio: π_b
- Compressor polytropic efficiency: e_c
- Turbine polytropic efficiency: e_t
- Burner efficiency: η_b
- Mechanical Shaft Efficiency: η_m
- Specific heat at constant pressure in the compressor: c_{pc}
- Specific heat at constant pressure in the turbine c_{pt}
- Ratio of specific heats in the compressor: γ_c
- Ratio of specific heats in the turbine: γ_t
- Lower heating value of fuel: h_{pr}

For a turboprop, a parametric cycle analysis yields the power output of the turboprop and the mass flow rate of fuel. Because all tests were performed with a static test bench, the PCA was performed with static inlet conditions. The PCA is performed by calculating the temperature and pressure inside the turbine engine through each set of components with the input quantities above. Station numbers are used in accordance with Aerospace Recommended Practice 755A [47]. For this analysis, the inlet mass flow rate, $\dot{m}_0$, is unknown and must be iterated until the expected power output matches the manufacturer's designed power output.

Total (stagnation) temperature and pressure can be calculated with the ratio of specific heat, the local mach number, M, and the static temperature or pressure (T, P) respectively (Equations 7&8)

$$T_T = T\left[1 + \frac{\gamma - 1}{2} M^2\right] \quad (7)$$

$$P_T = P\left[1 + \frac{\gamma - 1}{2} M^2\right]^{\gamma/\gamma - 1} \quad (8)$$

Because the test is performed at static conditions, total pressure and temperature at station 2 are equal to the ambient conditions.

$$T_{T2} = T_0 \quad (9)$$

$$P_{T2} = P_0 \quad (10)$$

The compressor pressure ratio can be used with the compressor polytropic efficiency to calculate the temperature ratio (τ) across the compressor (equation 11). The temperature ratio can be used to calculate the total temperature at station 3 (equation 12).

$$\tau_c = \pi_c^{\frac{\gamma_c - 1}{\gamma_c * e_c}} \quad (11)$$

$$T_{t3} = T_{t2}\tau_c \quad (12)$$

The fuel-air ratio (f) can be calculated using the burner efficiency, fuel lower heating value, T_{T3}, and T_{T4} (Equation 13). The Fuel-air ratio can then be used to calculate the mass flow rate of fuel using the inlet mass flow rate (Equation 14). $\dot{m}_{fuel}$ is a major outcome from the PCA, and can be used with the power estimation later in the analysis to predict BSFC.

$$f = \frac{c_{pt}T_{T4} - c_{pc}T_{T3}}{\eta_b h_{pr} - c_{pt}T_{T4}} \quad (13)$$

$$\dot{m}_{fuel} = f\dot{m}_0 \quad (14)$$

The high-pressure turbine is used to power the compressor. The power balance between the compressor and turbine can be seen in equation 15. This power balance can be rearranged to calculate the total temperature at station 4.5 (Equation 16).

$$\dot{m}_0 c_{pc}(T_{T3} - T_{T2}) = \eta_m \dot{m}_4 c_{pt}(T_{T4} - T_{T4.5}) \quad (15)$$

$$T_{T4.5} = T_{T4} - \frac{1}{(1+f)\eta_m}\frac{c_{pc}}{c_{pt}}(T_{T3} - T_{T2}) \quad (16)$$

T_{T4} and $T_{T4.5}$ can be used to calculate the temperature ratio across the high-pressure turbine (Equation 17). The temperature ratio and turbine polytropic efficiency can be used to calculate the pressure ratio across the high-pressure turbine (Equation 18).

$$\tau_{tH} = \frac{T_{T4.5}}{T_{T4}} \quad (17)$$

$$\pi_{tH} = (\tau_{tH})^{\frac{\gamma_t}{(\gamma_t - 1)e_t}} \quad (18)$$

The high-pressure turbine pressure ratio can be used with all other previous pressure ratios to calculate the total pressure at station 4.5 (Equation 19) and the total pressure at station 4.5 can be used to calculate the pressure ratio across the low turbine (assuming P_{T5} is equal to P_{T9}) (Equation 20). The low-pressure turbine pressure ratio can be with the turbine polytropic efficiency to calculate the low-pressure turbine temperature ratio (Equation 21). The low-pressure turbine temperature ratio can be used to calculate the total temperature at station 5 (Equation 22).

$$P_{T4.5} = P_{T2}(\pi_c \pi_b \pi_{tH}) \quad (19)$$

$$\pi_{tL} = \frac{P_{T5}}{P_{T4.5}} \quad (20)$$

$$\tau_{tL} = \pi_{tL}^{\frac{(\gamma_t - 1)e_t}{\gamma_t}} \quad (21)$$

$$T_{T5} = T_{T4.5}\tau_{tL} \quad (22)$$

The change in total temperature across the low-pressure turbine can be used to estimate the power extracted with the secondary turbine and available as shaft power (Equation 23). A negligible amount of thrust is produced by Kingtech turboprop exhaust, so jet thrust is not accounted for in the total energy output of the turboshaft. If electrical efficiency is known or otherwise assumed, it can be used to estimate the DC power output of the turboelectric system (Equation 24).

$$P_{shaft} = \dot{m}_4 c_{pt}(T_{T4.5} - T_{T5}) \quad (23)$$

$$P = \eta_e P_{shaft} \quad (24)$$

The power predicted with equation 24 can be used with the fuel mass flow rate predicted with equation 14 to estimate the BSFC of the system with equation 5.

Electric Motors and Generators

Electric motors and generators have complex static and dynamic responses. Optimized designs would involve careful consideration of electric motor behavior. For the turboelectric systems designed and tested for this research though, there are only a few key concepts that must be discussed to design turboelectric systems.

All the motors and generators utilized in both the turboelectric system and load are brushless DC motors. These motors provide flexibility as a brushless direct-current (DC) motor can be used as a generator and visa-versa. When used as a generator, there are 3 lines which come off the motor. Each line carries 1-phase of alternating-current (AC) power for a total of 3-phases. These power lines are then run through a solid-state full-wave bridge rectifier to transform the power into DC power. A photo of the 13-kW turboelectric system can be seen in Figure 10 with the generator and rectifier highlighted.

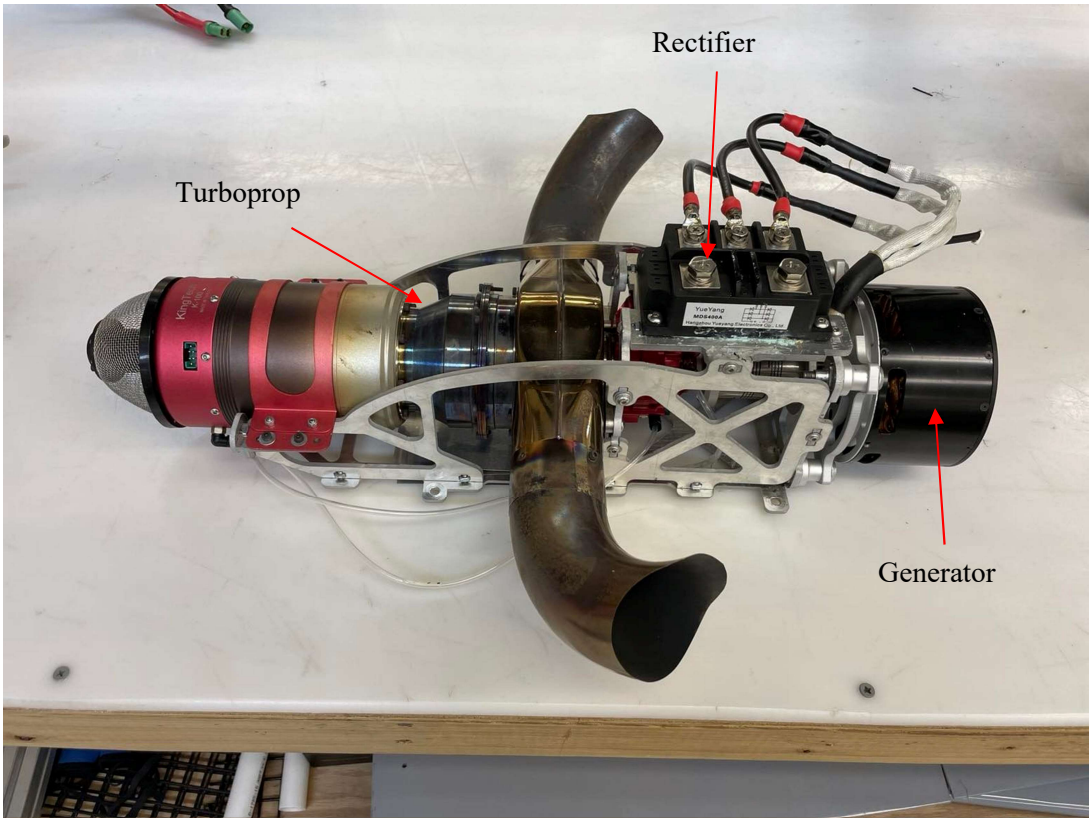

Figure 10. A photo of the 13-kW turboelectric system showing key components

Once power has been transformed from AC to DC, it can then be transmitted throughout the aircraft to any number of loads desired. The rectifier can act as a junction box for wires to be split off to the different electrical loads. For the tests performed, an electric motor with an attached propeller was used to better emulate the load drawn by an aircraft. Once the DC power is at the load motor, it must be sent through an electronic speed controller (ESC) to drive the motor. The ESC takes the DC power and transforms it back into either sinusoidal or square wave AC power (depending on motor speed). The AC power generated off the motor cannot be directly used to spin the load motor, because there is no way to ensure that the load motor is being driven in phase with its internal magnets. The ESC controls the load motor to ensure it is being properly driven in-phase.

Another key concept is the electric motor voltage constant, k_v. The voltage constant is determined by the physical configuration of the motor, including number of permanent magnets, number of windings in the stator, and the size of the motor. While there are some motors which are capable of actively changing their voltage constant, all the motors used in this experiment had a fixed k_v. Because these motors are COTS parts, the k_v is known from information given by the manufacturer. The voltage constant is important because it relates the voltage supplied to the motor to the RPM the motor would achieve said voltage with no external torque applied. This voltage(V)-speed (ω) correlation can be seen in equation 25.

$$\omega = Vk_v \tag{25}$$

This voltage constant also works for the reverse process and can be used to estimate the voltage produced by a generator at a certain RPM with no electrical load drawn.

The k_v value can inform about the voltage of a generators in a no-load state, but under real applications, the generator will be under load. Under load, the voltage supplied by the generator can sag as much as 20% below what the above k_v equation would predict. There are several reasons for this loss. The first cause of the lower voltage is due to simple ohmic losses within the

winding of the motor. Other losses come from added induction in the core of the motor. The third cause is from interactions between the magnetic field of the motor and the core of the motor.

It is important that the delivered power from the turboelectric system can be calculated from readily measurable quantities. Voltage and current can be readily measured in DC power lines with COTS measurement devices. More detail as to how this data is acquired will be discussed in the next chapter. The DC power transmitted through a circuit is simply the product of voltage and current (Equation 26):

$$P = VI \tag{26}$$

Ohmic losses in electrical equipment are a function of current. The power lost in an electrical system due to ohmic losses is proportional to the current squared. The power lost through ohmic losses is translated to a thermal load on the electrical components. Equation 27 shows the equation for power loss due to ohmic losses.

$$P_{loss} = I^2R \tag{27}$$

Control methodologies for the gas turbine engine

At all times current produced by a system is conserved, so to maintain steady operation, equal power must be produced and consumed. There are two general methodologies to ensure the power produced is matched to the power consumed:

- Directly throttle the turbine engine and configure the electrical load to use all power available to it
- Directly control the electrical load and design a controller to throttle the turbine to match the demanded power

The first methodology will be known as Direct Turbine Control (DTC) and the second methodology will be known as Active Turbine Control (ATC). A conceptual schematic of the DTC mode can be seen in Figure 11. In the DTC operating mode, the operator directly adjusts the

throttle sent to the Engine control unit (ECU). The electrical load is configured to run at maximum throttle. With the load set to be constantly at maximum throttle, the load will use any power it is provided. This mode is therefore a type of electrical passthrough where the power output from the turbine directly corresponds to the power usage of the electrical load. This means that in dynamic response, the DTC system behaves similarly to the turbine engine, as the turbine engine is the sole driver of the power output of the system.

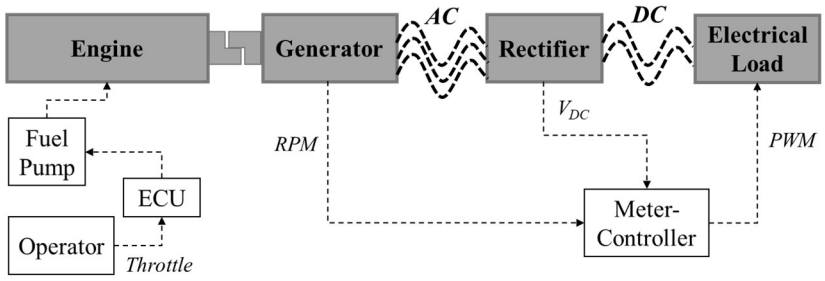

Figure 11. A schematic of the DTC operating mode

In the ATC operating mode, the operator directly throttles the electrical load, and a controller is configured to throttle the turbine to match the power needs of the load. In the ATC operating mode, a battery is included in parallel with the turboelectric system. A schematic of the ATC mode can be seen in Figure 12 showing all the key components. Like the DTC mode, the engine, generator, rectifier, and load are still in place alongside all the turbine support equipment (ECU and fuel pump). Notice that for the ATC mode, the throttle signal goes directly to the electrical load, and the controller is entirely responsible for sending throttle commands to the turbine engine.

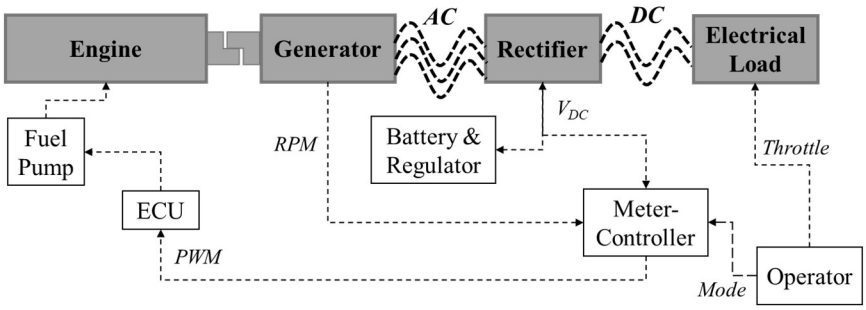

Figure 12. A schematic of the ATC operating mode

This battery serves two purposes within the ATC system. First, the battery can provide power augmentation. Power augmentation means that the battery can output power on top of what the turbogenerator can supply. Shorter takeoff distances can be achieved with the supplemental power of the battery. Power augmentation can also allow for a smaller turbogenerator to be used. Turboprop engines must usually be sized for the maximum power output, and this is often at takeoff or during other short portions of the flight (e.g., combat maneuvering). With power augmentation, a smaller turbine engine can be used that supplies only enough power for cruise condition, and the battery can supply the additional power needed during maximum-power scenarios (takeoff, combat maneuvering, aborted landings, etc.). The second purpose of the battery is to provide the possibility of quicker and smoother dynamic response of the turboelectric system. Batteries can provide near-instantaneous power output (on the order of milliseconds), while turbine engines have a slower response time to changes in throttle setting (on the order of seconds). The battery can provide power during the time between when the operator demands an increase in power and when the turbine reaches the desired power output. This also works in the reverse-case where the operator demands less power from the load. The battery can charge with the excess power provided by the turbine between when the load power demand is decreased and when the turbine reaches a lower power output. The use of a battery results in near-instantaneous response time and can reduce the occurrence of voltage spikes and drops during dynamic loading.

To throttle the turbine in response to the demanded power of the electrical load, there needs to be a way of estimating when the load is demanding more or less power. This is achieved with a controller measuring the voltage supplied on the rectifier block. When the load draws more power, more current is drawn from the turboelectric system. This higher current causes the voltage across the rectifier to drop for three reasons. First, the higher current results in a higher torque required to spin the generator, causing the output shaft of the turbine to spin at a lower RPM (resulting in a lower voltage output from the generator). Second, the voltage produced by

the generator sags as a response to ohmic, inductive, and magnetic losses as described above. Third, the voltage of the individual battery cells temporarily drops when high current is drawn from them. The opposite effect happens when there is almost now power demand. The current is low, therefore there is little torque on the generator, there are fewer losses within the generator, and the battery cells are sitting at their resting voltage. Therefore, measuring the voltage can give an indication of the power demand of the turboelectric system.

A PID controller was implemented on an Arduino microcontroller to drive the throttle of the turbogenerator. The PID was designed to take a measurement of the voltage across the rectifier block and output a PWM signal to drive the throttle of the turbogenerator. The PID was designed to keep the rectifier voltage at approximately 47-V. 47-V was selected because this is roughly half-way between the maximum charge (50.4-V) and nominal charge (44.4-V) of the 12-S LiPo battery. The 47-V setpoint ensured turbine would not output power if the battery was at a near-full charge and no load was being demanded but would output power if a high load was demanded or the battery was not at a high state of charge. Figure 13 shows a block diagram of the ATC scheme. This figure highlights what operations were performed on the microcontroller.

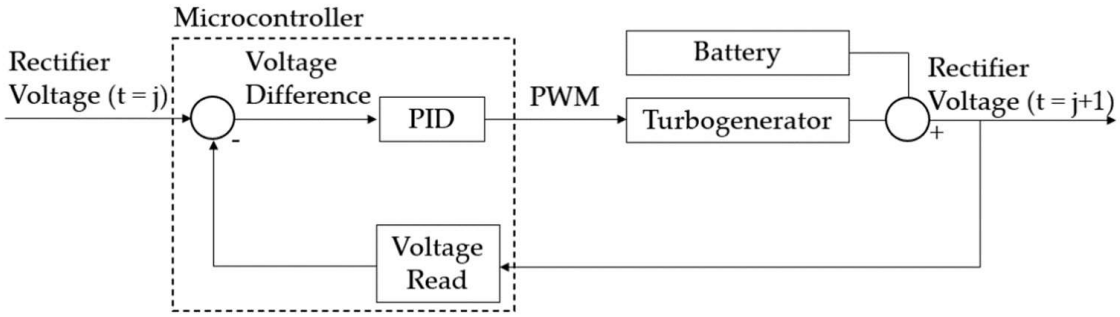

Figure 13. A basic control block diagram of the ATC controller.

CHAPTER III

Methodology

Experimental Setup

Turboelectric System

The usage of COTS parts has simplified the design and construction of the turboelectric systems used in testing. As discussed in the literature review, many other UAV-scale turboelectric systems are clean sheet-designs. While clean-sheet designs are excellent at reducing the weight of the turboelectric system, there is a lengthier development cycle as new designs for all components must be created and tested. The challenges of a clean sheet design can be seen in [38] where a turbine designed to produce 500-W of electrical power was only able to achieve 5-W in early tests. Purposefully designed turboelectric systems will be a necessity for commercial applications of a turboelectric system. The Kingtech Turboprop Turbine is a core element of the system. A K-45TP can be seen in Figure 14. These turbine engines were selected so that the power output shaft could be used to couple to and spin the generator. Kintech turbine engines are cheaper than the similar JetCat turbine engines, and therefore present a lower risk to budget than JetCat turbine engines in the event of an accident.

Figure 14. A photo of a Kingtech K-45TP

All 3 turboelectric systems were designed to produce voltage within the 12-S (39.6-50.4-V) voltage range. Therefore, a different generator was used with each size of turboelectric system (each with a different k_v). Photos of all three turboelectric systems can be seen in Figure 15.

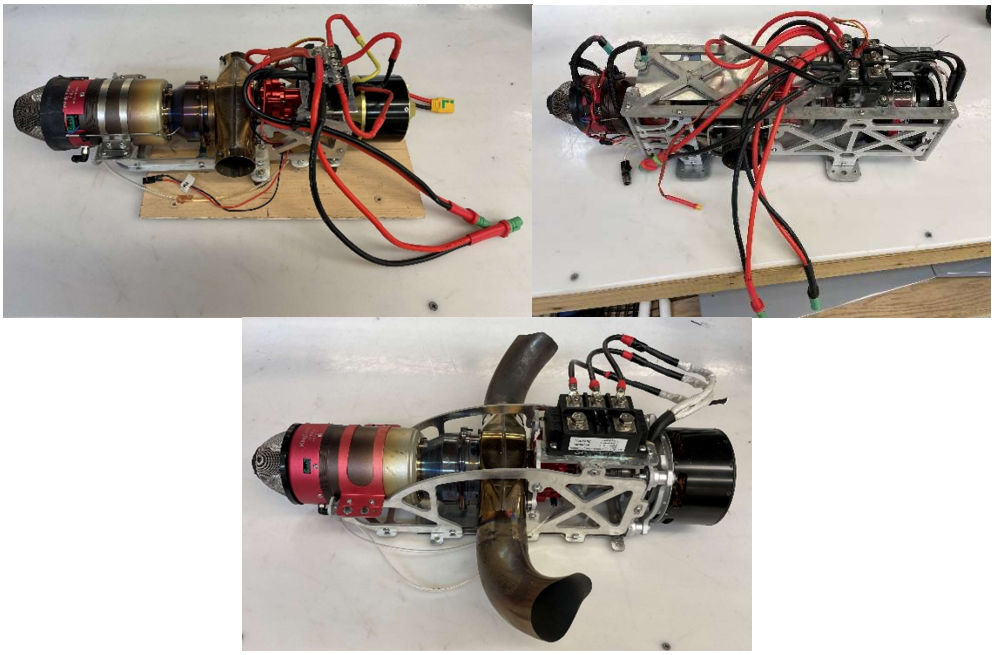

Figure 15. Left: the 5-kW turboelectric system, Right: the 7-kW turboelectric system, Center: the 13-kW turboelectric system

In aircraft applications, weight is always a key consideration because of the impact on aircraft performance and fuel usage, and many key performance metrics are scaled by power system

mass. The mass of all three studied turboelectric systems is shown in Table 1. For the DTC system, the weights includer were the turbine engine, shaft coupler, housing, rectifier, and generator for each system. The turbine engine, shaft coupler, housing, and rectifier all represent key components of the powertrain of the turboelectric system. Accessory hardware was not included in the weight because this study is focused primarily on the direct powertrain components. The total weight of accessory components can depend on several factors including capacity of batteries and control hardware used. The ATC system weight additionally includes the BMS, the switching circuitry, and the battery used. The battery weight provides some variability in the weight of the ATC system, as battery weight is driven by battery capacity. It is important to include the weight of the battery because it is providing some of the power output of the system. Because the ATC system includes additional weight with the battery system, and the battery system weight is variable, comparisons are best made within each type of system (i.e., only comparing DTC systems to other DTC systems and ATC systems to other ATC systems).

The 7-kW system is 76% heavier than the 5-kW system and only 11% lighter than the 13-kW system. The 7-kW system was the first produced, and thus had a bulkier housing for system safety. The 5-kW and 13-kW used less bulky housings with thinner aluminum. Further optimization could still be performed to bring housing weights down. The housing weight represents approximately 30% and 20% of the weight of the 5-kW and 13-kW systems respectively, while the housing weight represents 40% of the weight of the 7-kW system. If the 7-kW housing were similarly designed to the 5-kW or 13-kW housings, the housing would be approximately 25% of the weight of the 7kw System. Therefore, a lighter for housing for the 7-kW system could possibly bring the system weight down to around 5.7-kg (12.9-lbm).

Table 1.Turboelectric system mass

System	Mass
DTC 5-kW	4.2-kg (9.3-lbm)
DTC 7-kW	7.4-kg (16.4-lbm)
DTC 13-kW	8.4-kg (18.5-lbm)
ATC 5-kW	7.3-kg (16.2-lbm)
ATC 7-kW	10.6-kg (23.3-lbm)
ATC 13-kW	11.5-kg (25.4-lbm)

Test Bench

A static, ground test stand was designed and assembled to test the turboelectric system's capabilities and potential safety concerns, specifically dynamic loading. This bench test stand utilized an aluminum optical breadboard attached to a steel rolling table for ease of mobility and modularity. A 20 kW-rated electric motor, driving a three-blade propeller, and two separate five kW-rated electric ducted fans (EDFs) were chosen as the applied electric loads during the experiments. Electric motors pose a danger risk more severe than that of piston engines, as stated in [48]: "Model aircraft electric motors can be more dangerous than gas engines of the same power class because the propeller does not slow down readily when a body part is hit; rather, the motor just pulls more current from the battery as it attempts to retain the RPM." The 20 kW motor and corresponding propeller were housed within a wire-mesh assembly to ensure foreign objects could not impact the blades to help prevent injury during testing. The ground test stand provides a portable testbed that can be utilized for differing ranges of turboelectric systems, with a maximum overall power loading capability of 23 to 28 kW. A photo of this system can be seen in Figure 16.

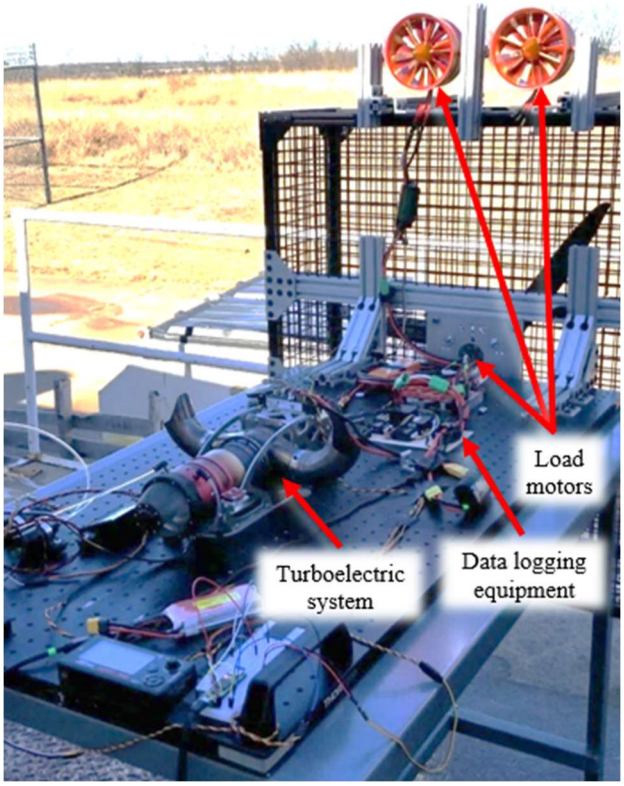

Figure 16 A photo of the bench test stand with the K-60TP-based system installed, showing the available electric loads of the 28 in. propeller motor and two additional five kW EDFs.

Voltage and current produced by the generator were monitored and logged to provide real-time power production values of each system. The power produced was calculated using voltage and current values measured by the Mauch Power Module in Table 2. This power module was placed in-line between the turboelectric system and the electric load (motor). This hall effect sensor package designed to monitor voltage and current data can be seen in Figure 17. Power was calculated from the measured voltage and current values. Turbine throttle data and turbine fuel consumption rate were also observed in real-time to help ensure the turbine was not operating in a dangerous regime (e.g., operating at too high of a voltage).

Table 2. Test Equipment

TEST EQUIPMENT	MANUFACTURER AND MODEL
Turbine Engines	K45TP (5 kW), K60TP (7 kW) & K100TP (13 kW)
Generators	Great Planes 50cc (230 Kv), Turnigy Rotomax 100cc (167 Kv), Off-The-Grid 20 kW (130 Kv)
Rectifier	200 Amp, 3-Phase, Full-Wave Bridge Rectifier
Power Module	Mauch 200 Amp Power Module
Data Recorder	Pixhawk 2 Flight Controller, 400 Hz Sampling Rate
Temperature Sensor Recorder	Teensy 3.5
Electronic Speed Controller	Trampa Boards 75 V, 300 Amp Vedder ESC
Electric Load Motor	Off-The-Grid 20 kW, 100 Kv

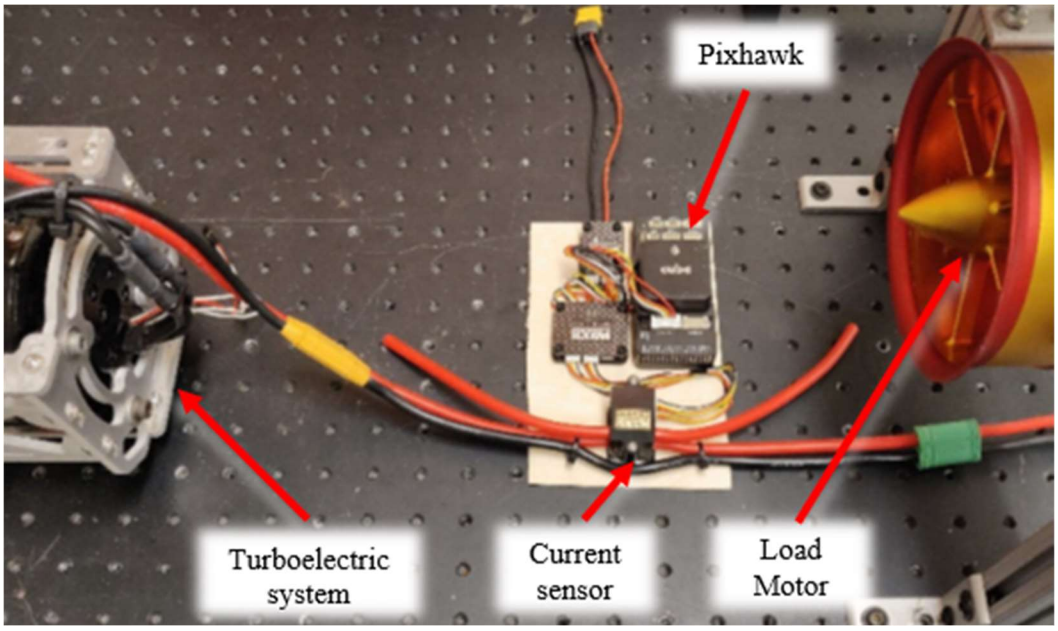

Figure 17. A photo of the Mauch power module used to measure voltage and current between the turboelectric system and the load. (Both lines were used during testing).

Procedure

Steady State

Initial setup involved wheeling the test cart outside to a safe test area at the OSU Richmond Hill Research Complex. All electrical connections were checked to ensure that all proper wirings between the turboelectric system, current sensor, and load were made. In addition, all signal wires between devices such as the turbine engine control unit (ECU), turbine engine, receiver, and load

motors were checked to ensure all were connected. The fuel tank was then filled to maximum with Jet-A. The Pixhawk and current sensors were powered on, and the time was marked down to assist in finding test data within the Pixhawk log files. It is at this point that the Pixhawk began recording voltage and current data. The turbine engine was sent a start command and allowed to run through its pre-programmed startup sequence. If the DTC systems were being tested, the electric load was sent a continuous maximum throttle signal (to ensured that the electric load was configured such that it would take any power the turboelectric system can output). After sitting at idle, the throttle was changed to the desired throttle setting. The turbine engine was allowed to respond and rest at the desired throttle setting for 15- to 30-seconds to ensure the system had reached steady state. After steady state was reached, a timer was started, and the initial fuel weight was recorded. After 30-seconds a mid-test fuel weight was recorded, and then after 60-seconds the final fuel weight was recorded. After the 60-second test was completed, the turbine was taken back to idle for 1- to 2-minutes before beginning the next test. The process of changing the system throttle, waiting, and recording data was repeated for all the test points of each system. If the system was running low on fuel, the turbine was shut down, and a note was made on the fuel data collection sheet, the fuel tank was refilled, the turbine was restarted, and then tests would resume where they left off.

Each of the three different turboelectric systems were tested in both ATC and DTC modes at five different throttle settings: 0%, 25%, 50%, 75%, and 100%. The tests were performed from the highest throttle setting (100%) to the lowest (0%). Upon the completion of all the test points for one system, data was retrieved from the Pixhawk, the completed turboelectric system was removed, and the next system was installed.

Transient

A similar startup procedure was used for the transient tests. Once the system was setup and the turboelectric system had reached idle, the system throttle was moved to the initial test point. Once

the system reached the initial test point, the system was kept at that throttle setting for 15-30-s. After the 15-30-s had passed, the throttle was rapidly moved to end state of the first test (e.g., the throttle was moved from 50% to 75%). Once the throttle was moved to the end state throttle setting, the system was then kept at the end throttle setting for 15-30-s to ensure the system had reached steady state at the new throttle setting. The throttle was then moved to the initial throttle setting for the next text and the process was repeated for each test point. This process was repeated for all systems in both ATC and DTC modes. The test points were as follows:

50% to 75%

75% to 100%

50% to 100%

100% to 50%

100% to 75%

75% to 50%

Parametric Cycle Analysis Predictions

A PCA was performed for each of the 3 turboprop engines to estimate the power output and BSFC before tests were performed. This PCA was performed to set BSFC expectations for the experiments and grant some trust in the results. The same fluid properties were used for all 3 turbine engines and their values can be seen in Table 3. Static sea level standard day conditions were used for ambient conditions.

Table 3. Fluid properties for PCA

Property	Value
P_0	14.7-psi
T_0	59°F
c_{pc}	0.24-BTU/lbm-R
c_{pt}	0.276-BTU/lbm-R
γ_c	1.4
γ_t	1.33
h_{pr}	18400-BTU/lbm

K-45TP

The necessary inputs for the PCA were benchmarked or estimated. Their values can be seen below in Table 4. Engine performance values such as polytropic and burner efficiencies were retrieved from Elements of propulsion [46]. Level of Technology 1 was assumed for all components except for the compressor and turbine which were assumed to be Level of Technology 2. The electrical efficiency estimated in Moody et al. is used here (77%). Calculations were performed as described in the theory section and results are presented in Table 5.

Table 4. K-45TP PCA inputs

Parameter	Value
T_{T4}	1111-K (2000-R)
π_c	1.8
π_b	0.9
e_c	0.85
e_t	0.85
η_b	0.88
η_m	0.95
η_e	0.77
$\dot{m}_0$	0.15-kg/s (0.331-lbm/s)

Table 5. K-45TP PCA results

Parameter	Value
Power	3900-W (5.3-hp)
BSFC	3.5-kg/kW-hr (5.8-lbm/hp-hr)
PWR	0.096-kW/N (0.57-hp/lbf)

K-60TP

The PCA inputs for many of the values of the K-60TP were the same as for the K-45TP. The primary differences are the compressor pressure ratio. The PCA inputs can be seen in Table 6 and the results can be seen in Table 7. As expected, the higher compressor pressure ratio results in a higher thermal efficiency, giving the K-60TP a lower expected BSFC. The predicted PWR of the 7-kW system is lower than that of the 5-kW system. This is because of the increased weight of the 7-kW housing. If the housing were made lighter (as discussed previously) the PWR could potentially be brought up to 0.096-kW/N, matching the PWR of the 5-kW system.

Table 6. K-60TP PCA inputs

Parameter	Value
T_{T4}	1111-K (2000-R)
π_c	2.0
π_b	0.9
e_c	0.85
e_t	0.85
η_b	0.88
η_m	0.95
η_e	0.77
$\dot{m}_0$	0.15-kg/s (0.331-lbm/s)

Table 7. K-60TP PCA results

Parameter	Value
Power	5500-W (7.3-hp)
BSFC	2.5-kg/kW-hr (4.1-lbm/hp-hr)
PWR	0.075-kW/N (0.45-hp/lbf)

K-100TP

Like the K-60TP, the K-100TP uses many similar assumptions to the other engines. The primary differences are the compressor pressure ratio and $\dot{m}_0$. The inputs are shown in Table 8 and the results are shown in Table 9. As expected, the K-100TP has the lowest predicted BSFC of all 3 systems.

Table 8. K-100TP PCA inputs

Parameter	Value
T_{T4}	2000-R
π_c	2.1
π_b	0.9
e_c	0.85
e_t	0.85
η_b	0.88
η_m	0.95
η_e	0.77
$\dot{m}_0$	0.551-lbm/s

Table 9. K-100TP PCA results

Parameter	Value
Power	10000-W (13.7-hp)
BSFC	1.7-kg/kW-hr (2.8-lbm/hp-hr)
PWR	0.126 kW/N (0.75-hp/lbf)

Comparison to other electrified propulsion

While this study focuses on the performance of turboelectric systems, it is important to understand how the performance of these systems compares to other forms of electrified propulsion. An example of a commercially available piston-hybrid power system for unmanned aircraft is the Harris Aerial H5000 generator [1]. Table 10 shows the performance as claimed on Hariss Aerial's website for the H5000. The BSFC of the H5000 is less than half that of the lowest predicted turboelectric system (the 13-kW system). This means that the H5000 will burn roughly ½ as much fuel per unit power compared to the 13-kW system. However, the lowest power to

weight ratio predicted for the turboelectric systems (the 7-kW system) is roughly 1.75x higher than that of the H5000. The 13-kW system has a predicted power to weight ratio almost 3x higher than the H5000.

Table 10. Performance of the Harris Aerial H5000 generator

Parameter	Value
Power	4300-W (5.8-hp)
Mass	10-kg (22-lbm)
BSFC	0.86-kg/kW-hr (1.41-lbm/hp-hr)
PWR	0.044-kW/N (0.26-hp/lbf)

Current LiPo batteries have a specific energy up to 265-W-h/kg [49]. Meanwhile Jet fuel has a specific energy of 11900-W-h/kg[46]. The full specific energy of the Jet fuel cannot be realized due to losses within the turbine engine and the electrical system. The thermal efficiency of the 5-kW system is approximately 15%. Combining the thermal and electrical efficiency, the efficiency of the turboelectric powertrain is predicted to be approximately 12%, meaning that the jet fuel would have a realized specific energy of around 1430-W-h/kg. The realized specific energy of the jet fuel for the turboelectric system is around 5.4x higher than that of LiPo batteries, without accounting for any of the electrical losses within a battery-based system.

CHAPTER IV

Results

Steady State Performance

DTC Performance

As described above, during steady state tests, the turboelectric systems were started, allowed to idle, then taken to the desired throttle setting. These tests were divided between DTC and ATC operating modes. Fuel data was tabulated from the tests, and power data was retrieved from the data acquisition Pixhawk. Data from the Pixhawk included voltage and current data sampled at 10 times a second. The time at which tests occurred was taken down during the experiment and used to identify tests within the data. Data was averaged over 1 minute (600 samples). Average values and standard deviation were calculated. An example of the current and voltage data from a DTC steady state test can be seen in Figure 18. In Figure 18, around 2545-s you can see that the voltage begins to spike as the operator throttled up the turbine with only a small load. As the operator throttled up the electrical load, more current was generated and sent to the load. The voltage lowed as the current rose due to the voltage sag of the generator. Eventually this reached steady state as the electrical load was taken to full throttle and the turbine reached its operating throttle. This steady state area is where voltage and current data was taken from and was the time

during which the fuel data was recorded. The slope down the right side of the steady state section shows where the turboelectric system was throttled down.

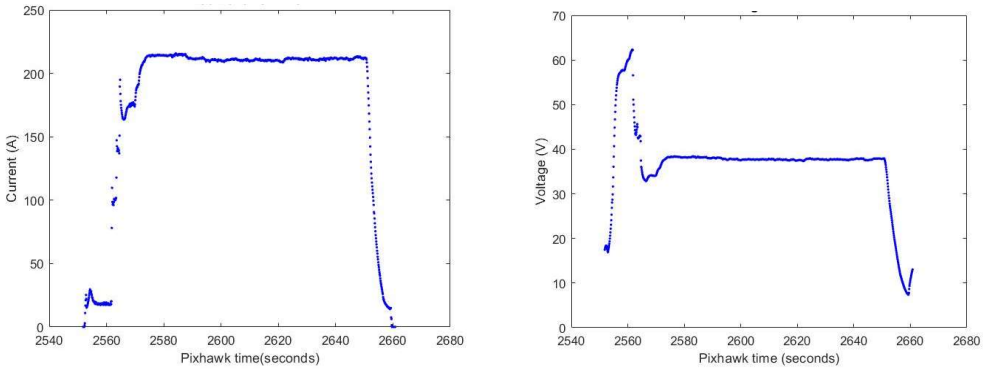

Figure 18. An example of current (left) and voltage (right) acquired from the Pixhawk during the 100% throttle test of the DTC 13-kW system

Figure 19 shows the power output of all three DTC turboelectric systems at 0%-100% throttle settings. Delivered power was calculated from the voltage and current data as described in the theory section. Standard deviations for power were calculated using the standard deviation of current and voltage. Error bars have been added to show the standard deviation of the measurement at each throttle point. The DTC 5-kW system produced approximately 0.6-kW at idle and showed a linear increase in power output up to approximately 3.0-kW with a slope of 25-W per percent throttle. The maximum of 3.0-kW is approximately 58% of the of the rated shaft output (5.2-kW) of the K-45TP. The DTC 7-kW system had an idle power of approximately 100-W and achieved a maximum power output of 5.6-kW. The linear fit had a slope of 54-W per percent throttle. The DTC 7-kW system delivered approximately 77% of the rated shaft power output of the K-60TP (7.3-kW), an improvement of almost 20% over the DTC 5-kW system. The DTC 13-kW system had an idle power of approximately 80-W and achieved a maximum power output of approximately 8.0-kW. 8-kW is approximately 61% of the rated shaft power output of the K-100TP (13-kW), 16% less than the DTC 7-kW system. The lower performance seen in both the DTC 5-kW and DTC 13-kW systems is likely due to the electrical component matching between the power turbine, generator, rectifier and/or electrical load.

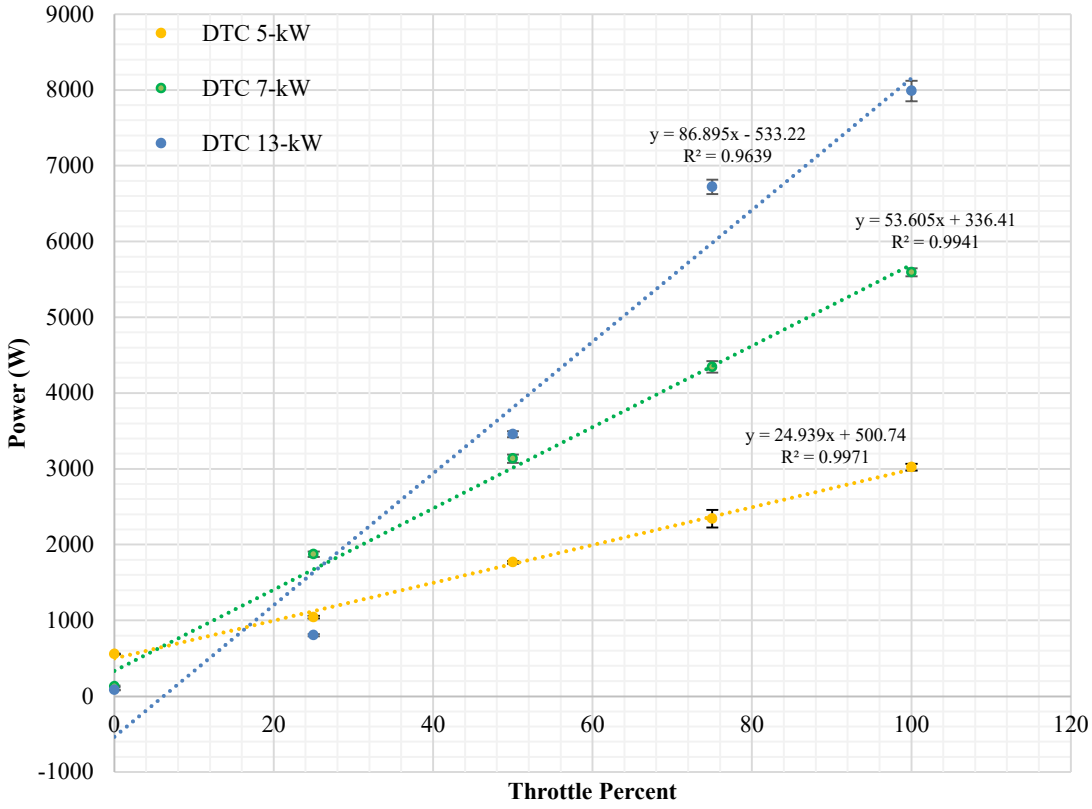

Figure 19. Trend in power output for the DTC turboelectric systems with linear fits

Figure 20 shows the trend in BSFC for all three DTC systems. Like larger turboprop engines, the BSFC decreases as the throttle increases for all three turboelectric systems. This decrease in BSFC is because of increased compressor pressure ratio leading to higher thermal efficiencies The 5-kW system achieved a minimum BSFC of 6.4-lbm/hp-hr at full throttle. The idle BSFC (17.3-lbm/hp-hr) was not included for consistency between the BSFC plots. The 7-kW and 13-kW systems had extremely high BSFC at their idle throttle (above 70-lbm/hp-hr). A 3-rd order polynomial trendline is displayed on this figure. Like the DTC 5-kW system, the BSFC decreases as the throttle increases. The DTC 7-kW system reached a minimum BSFC of 3.9-lbm/hp-hr at full throttle, a 39% improvement of the DTC 5-kW system. Like the DTC 5-kW and 7-kW systems, the BSFC decreases as the throttle increases. However, the BSFC curve appears to level at about 80% throttle, whereas it was not clear that BSFC leveled at even 100% throttle for the 5-kW and 7-kW systems. This is significant for mission planning purposes, indicating that BSFC

could be reasonably constant over a wide throttle range. The DTC 13-kW system reached a minimum 3.6-lbm/hp-hr (2.2-kg/kW-hr) BSFC at full throttle, which is a 7.7% improvement over the K-60TP system and a 43.8% improvement over the DTC 5-kW system. This reveals a non-linear scaling effect over this range of turboelectric systems with a decreasing rate of improvement as scale increases. So, as the turbine output power specification increased by 33% from the DTC 5-kW system to the DTC 7-kW system, the BSFC improved nearly 40%; however, as the turbine output power specification increased by 122% from the K-45TP to the K-100TP, the BSFC improved 44%, only 4% more than the DTC 7-kW system. Therefore, there is a diminishing benefit in BSFC as the engine scale increases. There is a notable effect at the lower throttle settings for the DTC 13-kW system, where the BSFC deviates to a much higher level than the DTC 5-kW or DTC 7-kW system. The results at lower throttle settings are less conclusive because small deviations in power are amplified when normalizing by a small magnitude. At the lower throttle settings, the fuel mass flow rate term is small, and is used to normalize the power output, which amplifies the small deviations in power. Small variations in power output can come from several effects including programming of the ECU, differences in electrical efficiency due to different voltages, and differences in thermal efficiency when performing off design.

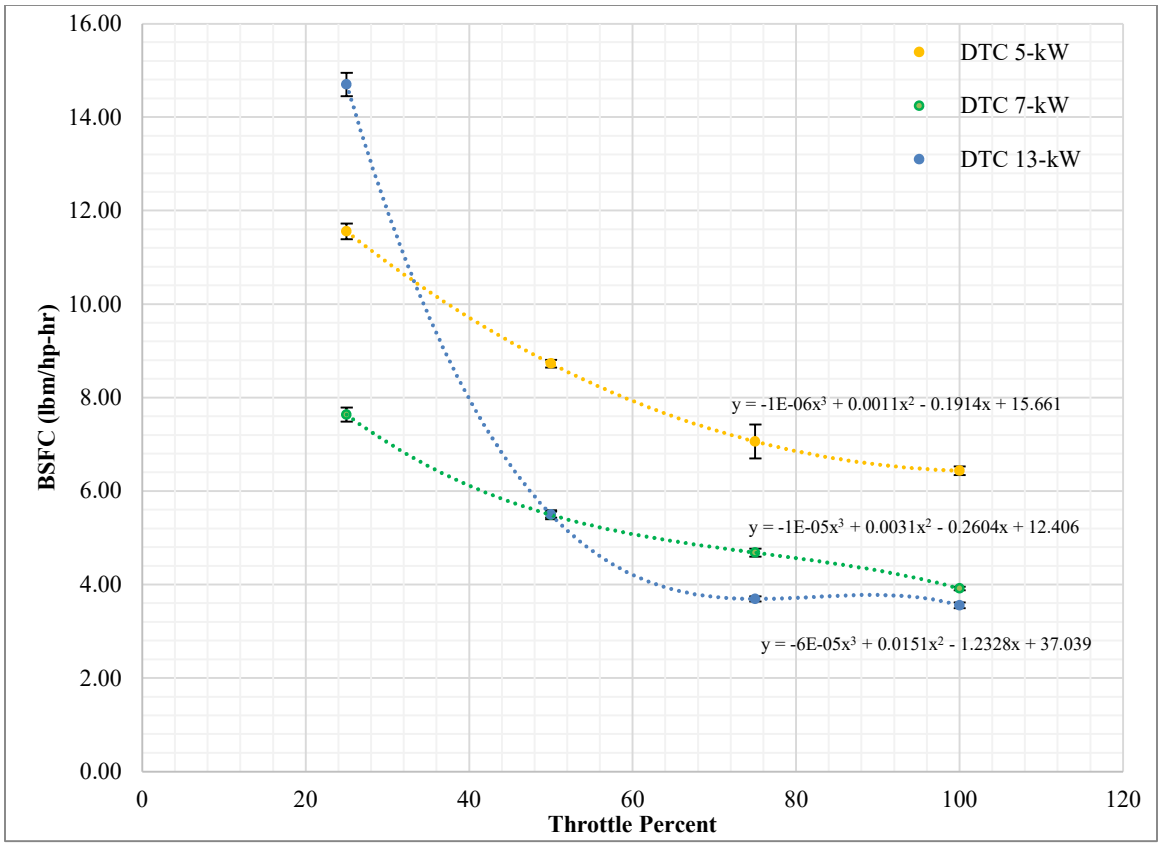

Figure 20. Trend in BSFC data for the DTC turboelectric systems with a third order polynomial fit

Voltage, voltage standard deviation, current, current standard deviation, and power for the three DTC systems are shown in Table 11 through Table 13. All three turboelectric systems show decreasing BSFC with increasing throttle point, as expected. Jet engines generally show a decrease in BSFC at higher throttle settings because of the corresponding increase in compressor pressure ratio and, consequently, increased thermal efficiency. The DTC 5-kW and DTC 7-kW systems operated most efficiently at 100% throttle, whereas the DTC 13-kW system achieved best BSFC at 75% and 100% throttle. The DTC 5-kW system showed higher BSFC than the DTC 7-kW and DTC 13-kW systems. This higher BSFC is likely due to the lower compression ratio of the K-45TP compared to the other turboprops, or that the generator used on the K-45 applied too much torque to the turboprop and therefore did not allow the output shaft to spin at its optimal RPM. The DTC 13-kW system showed the lowest BSFC of all three, achieving a 3.6 lbm/hp-hr

(2.2 kg/kW-hr) BSFC; however, it was not significantly improved over the 7-kW system. As expected, the DTC 13-kW system showed the highest rectified power output of all three turbines, with a maximum DC power of approximately 8-kW, but it appeared to have lower system efficiency compared to the DTC 7-kW system, based on manufacturer specified turbine output power.

Table 11. Summary of DTC 5-kW Turboelectric performance at different throttle settings

Turbine Throttle (%)	Current (A)	Current Standard Dev. (A)	Voltage (V)	Voltage Standard Dev. (V)	Power (W)	BSFC lbm/(hp*hr)
100	81.7	1.01	37.0	0.277	3024	6.4
75	69.4	2.73	33.8	0.979	2344	7.1
50	58.5	0.46	30.2	0.153	1768	8.7
25	41.6	0.48	25.2	0.210	1045	11.6
0	28.1	0.29	19.8	0.108	556	17.3

Table 12. Summary of DTC 7-kW Turboelectric performance at different throttle settings

Turbine Throttle (%)	Current (A)	Current Standard Dev. (A)	Voltage (V)	Voltage Standard Dev. (V)	Power (W)	BSFC lbm/(hp*hr)
100	144.2	1.215	38.8	0.183	5595	3.9
75	114.7	2.000	37.9	0.055	4347.1	4.7
50	84.3	1.449	37.2	0.039	3136.0	5.5
25	51.5	0.998	36.4	0.029	1874.6	7.6
0	3.7	0.290	35.3	0.015	130.6	70.2

Table 13. Summary of DTC 13-kW Turboelectric performance at different throttle settings

Turbine Throttle (%)	Current (A)	Current Standard Dev. (A)	Voltage (V)	Voltage Standard Dev. (V)	Power (W)	BSFC lbm/(hp*hr)
100	211.2	2.87	37.8	0.366	7987	3.6
75	189.4	2.34	35.5	0.239	6721	3.7
50	124.6	1.30	27.8	0.1383	3459	5.5
25	50.5	0.70	16.0	0.146	807	14.7
0	9.0	0.30	9.2	0.153	83	78.2

The maximum power produced by each system was used to calculate the maximum power-to-weight (PWR) ratio. These values are summarized in Table 14. The DTC 5-kW and DTC 7-kW

are very close to one another in terms of power to weight ratio, though the DTC 7-kW achieved only a slightly higher PWR due to the heavier housing. This is interesting because the DTC 7-kW system is significantly heavier than the DTC 5-kW system (approximately 1.7 times heavier). In comparison however, the DTC 7-kW system also produced approximately 1.8 times more power than the DTC 5-kW system. As discussed, the DTC 5-kW could potentially achieve a higher power output with a motor that would put less torque on the turbine. The DTC 13-kW system achieved the highest PWR of all three systems. This is expected, as the DTC 13-kW system was only 1.1 times heavier than the DTC 7-kW system, but output 1.4 times greater. The impact of these relationships affects propulsion and airframe integration, such that a designer should consider trade-offs in size, weight, power, and efficiency when selecting an appropriate turboelectric system for a given platform and mission.

Table 14. Maximum power-to-weight ratio of each DTC turboelectric system.

System	PWR (hp/lbf)	PWR (kW/N)	Uncertainty ± (hp/lbf)
DTC 5-kW	0.44	0.073	0.006
DTC 7-kW	0.46	0.076	0.004
DTC 13-kW	0.58	0.097	0.010

Uncertainty

Uncertainty was addressed by calculating the standard deviation for voltage and current during the steady state run, which was used to calculate the standard deviation for the derived quantities (power, BSFC, and PWR). Error bars showing one standard deviation were included on the above plots. Fuel weight was taken as an average value over the test, so this value was treated as a constant for the BSFC standard deviation. There were not multiple test points that could be used to calculate the standard deviation of fuel weight. Similarly, system mass was treated as a constant for the PWR standard deviation. While standard deviation is higher for some test points in the above plots (e.g., the 75% test point for the DTC 5-kW system), all show that there is no

overlap between any of the three system's uncertainty at any test point. The same method was used to address uncertainty for the ATC tests and is discussed in the results below.

ATC Performance

Slightly different behaviors were seen when the ATC scheme was used. This is because a battery was included in the loop. When a battery is included in the loop, power can come from both the turbogenerator and the battery. As discussed in the theory section, the turbine engine controller is designed with a setpoint around 47-V, meaning with a low power demand, the turbogenerator can recharge the battery. When the load is throttled to higher setting, it is demanding more power than just the turbogenerator can provide and power flows from both the battery and turbogenerator to the load. As the battery depletes, its voltage begins to decrease as does the power provided. An example of this power drop can be seen in the left side of Figure 21. The left side of Figure 21 shows the 5-kW system being run at 100% throttle, while the right side shows the 5-kW system run at 25% throttle. The left side shows that after some initial transience, around the 50-second mark, the K-45 was settled into steady operation. From this point the voltage continues to drop as energy is depleted from the battery. There is approximately a 1-V drop in the provided power over the minute long test. Meanwhile, in the right side of the figure shows that the voltage provided was relatively constant over the test. The voltage is more constant over the test because the battery is barely discharging unlike in the 100% throttle test. This can be seen in the voltage and current data from the BMS. Figure 22 Shows the BMS current and voltage data from the ATC 5-kW 100% throttle test. The same (approximately 1-V) voltage drop seen in Figure 21 can be seen in the BMS voltage data during the steady state test. The steady state portion of the test is from the 40-s mark to the 100-s mark in Figure 22. During this test up to 46-A was pulled from the battery. Figure 23 shows similar BMS data from the ATC 5-kW 25% throttle test, including similarly scaled axes. The steady state test ran from approximately the 30-second mark to the 80-second mark, and the current supplied from the battery was only around 2-A during the steady

state portion of the test. Unlike the 100% throttle test, almost no voltage drop can be seen. This is because of the small current coming from the battery, leading to very little depletion of the battery. Because of the larger voltage drop at higher power outputs, a higher standard deviation can be seen at the 75% and 100% throttle settings of all 3 turboelectric systems.

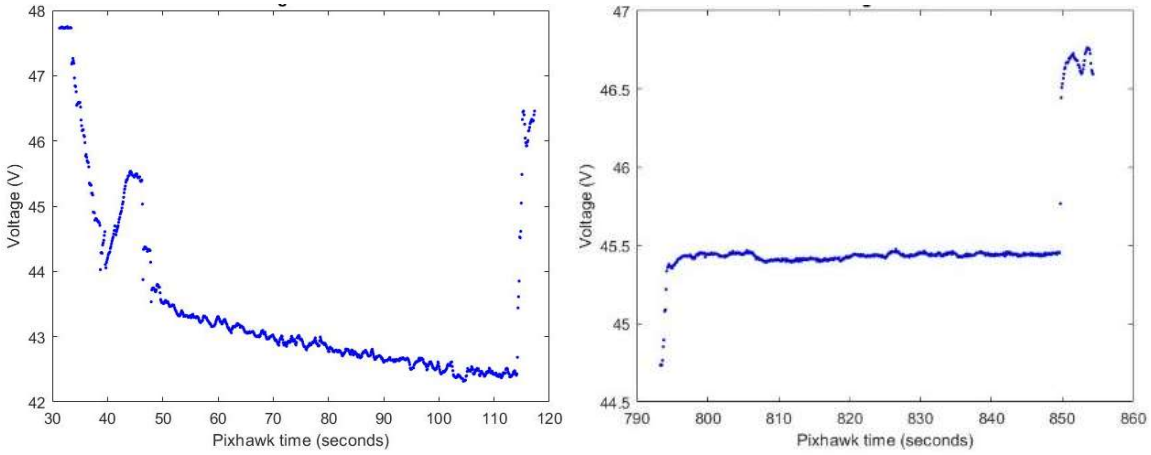

Figure 21. K-45 ATC Voltage Drop. (left) The voltage of the ATC 5-kW system at 100% throttle showing a voltage decrease as the battery depletes. (Right) The voltage of the ATC 5-kW system at 25% throttle showing no notable voltage drop.

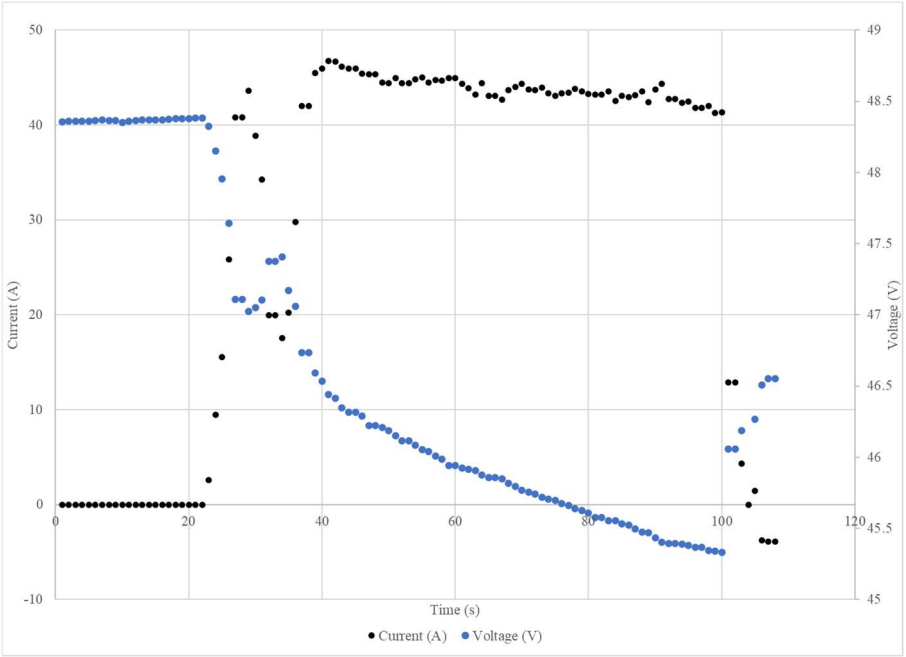

Figure 22. Data from the BMS showing current and voltage from the ATC 5-kW 100% throttle test

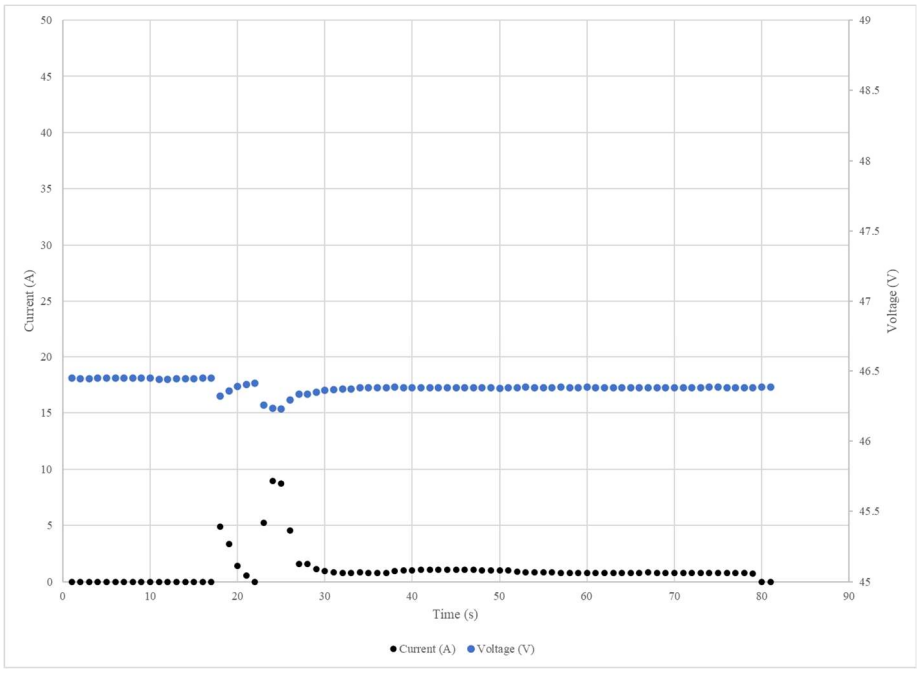

Figure 23. Data from the BMS showing current and voltage from the ATC 5-kW 25% throttle test

Figure 24 shows the trend in power produced by the three ATC systems. The ATC 5-kW system showed that almost no power was delivered at 25% throttle. The power delivered remained low at 50% throttle. Both at 25% and 50%, the delivered power was lower than the power produced in the DTC tests. The exact cause of the near-zero power output at 25% throttle is not known and was not seen in the ATC 7-kW or 13-kW tests. Data from the BMS in Figure 23 shows that the battery was discharging during the 25% throttle test of the ATC 5-kW system, so the low power delivered to the load was not due to power being diverted to charging. The highest power output of the ATC 7-kW system was at 75% throttle. The standard deviation of the power data at 75% and 100% was much higher than at the lower throttle settings. The cause for the higher standard deviation was discussed above. At higher throttle settings, more power is being drawn from the battery, resulting in a voltage drop throughout the test. As intended, the ability of the load to consume power far outstripped the ability of the turboelectric system to produce power. It is therefore likely that at both 75% and 100% throttle, the turbogenerator was driven to maximum throttle by the active controller, resulting in the steady state performance being mostly determined

by the battery's performance. The difference in power between the 75% and 100% test was approximately 300-W. Figure 24 also shows the trend in the ATC 13-kW system. Unlike the 7-kW system, the 13-kW system could supply almost all the required power with only the turbogenerator at 75% throttle. Therefore, the linear fit for the ATC 13-kW system has a squared value of the correlation coefficient is significantly lower than for the other two turboelectric systems

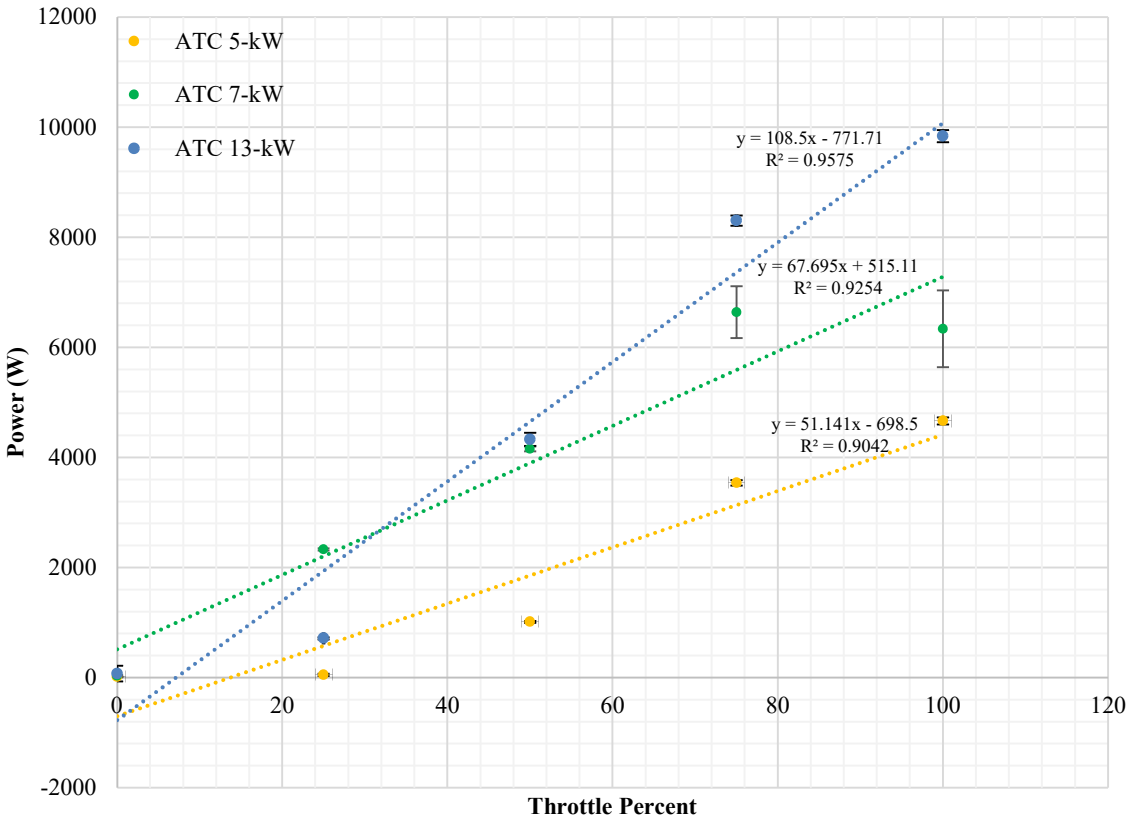

Figure 24. Trend in power output for the DTC turboelectric systems with linear fits

The BSFC data for the three ATC turboelectric systems can be seen in Figure 25. The BSFC of the ATC 5-kW system at 25% throttle is significantly higher than the other data points for the system (roughly 180-lbm/hp-hr). The BSFC at 25% throttle is not shown as it is plotted beyond the limit of the ordinate axis. This high BSFC at 25% throttle is due to the low amount of power produced (as discussed in Figure 24). The exact cause of this is not known. Like other systems

though, the BSFC of the ATC 5-kW system decreased at higher throttle settings, reaching a minimum of 3.9-lbm/hp-hr. The Trend in the data of the ATC 7-kW turboelectric system shows a slight difference in trend when compared to all the other turboelectric systems. The ATC 7-kw system achieved the lowest BSFC at 75% throttle rather than at 100% throttle. The minimum BSFC achieved was 3.5-lbm/hp-hr. At 100% throttle the ATC 7-kW system had a BSFC of 3.8-lbm/hp-hr. The error bars in the figure show that the uncertainty of the BSFC at 100% throttle for the ATC 7-kW system overlaps the BSFC of the ATC 5-kW system. The BSFC for the two systems at peak throttle is therefore not significant. The BSFC curve of the ATC 13-kW system is much flatter at 75% and 100% compared to the other turboelectric tests. A BSFC of 3.7-lbm/hp-hr was recorded at 75% throttle and a BSFC of 3.6-lbm/hp-hr was recorded at 100% throttle.

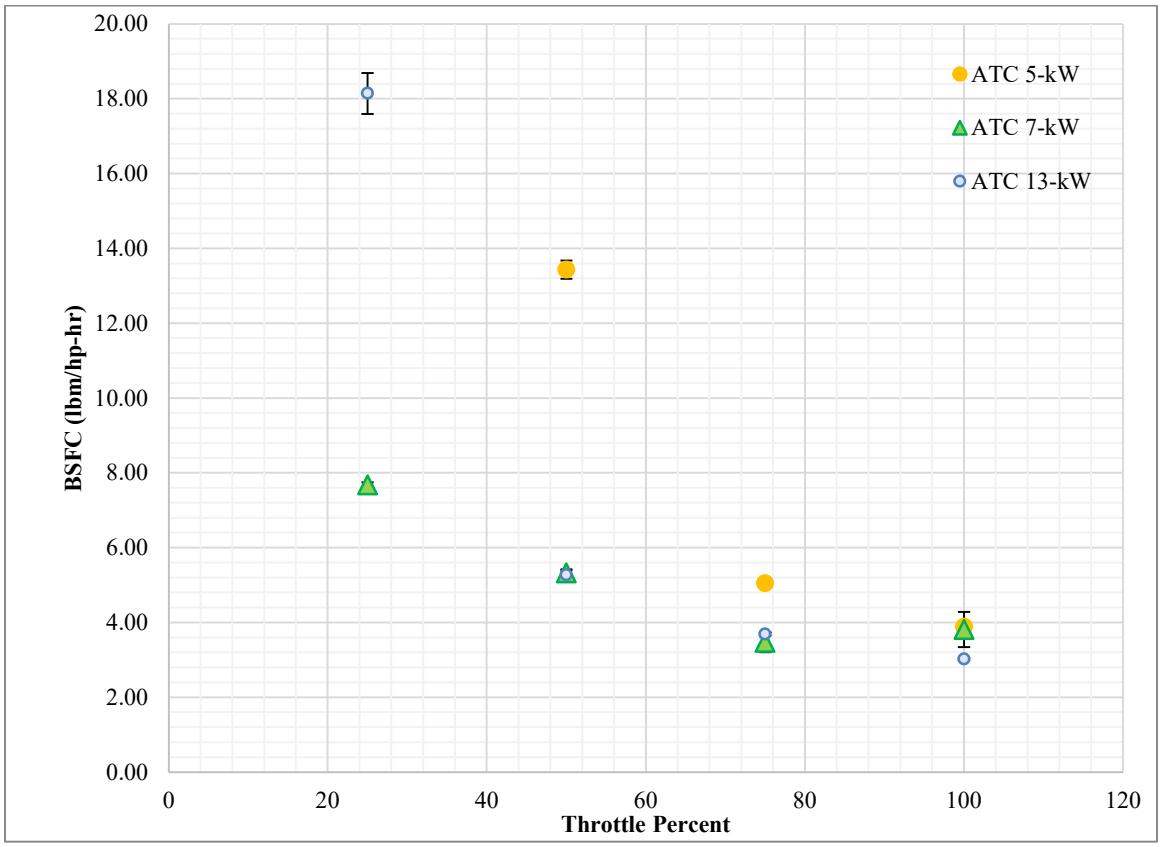

Figure 25. Trend in BSFC data for the DTC turboelectric systems

Voltage, voltage standard deviation, current, current standard deviation, and power for the three ATC systems are shown in Table 15 through Table 17. As discussed in the charts above, the ATC 5-kW and ATC 13-kW systems achieved their minimum BSFC at maximum throttle while the ATC 7-kW system achieved its minimum BSFC at 75% throttle. The ATC 13-kW system had the highest power output from any test reaching a power output of 9.8-kW.

Table 15. Summary of ATC 5-kW Turboelectric performance at different throttle settings

Turbine Throttle (%)	Current (A)	Current Standard Dev. (A)	Voltage (V)	Voltage Standard Dev. (V)	Power (W)	BSFC lbm/(hp*hr)
100	108.9	1.25	42.8	0.296	4666	3.9
75	80.8	1.12	43.9	0.109	3541.6	5.1
50	21.8	0.33	46.5	0.4511	1015.8	13.4
25	1.1	0.43	45.7	0.508	50.5	181.6
0	0.4	0.18	45.9	0.318	18.9	260.8

Table 16. Summary of ATC 7-kW Turboelectric performance at different throttle settings

Turbine Throttle (%)	Current (A)	Current Standard Dev. (A)	Voltage (V)	Voltage Standard Dev. (V)	Power (W)	BSFC lbm/(hp*hr)
100	170.2	18.60	37.3	0.398	6338.4	3.8
75	173.8	12.29	38.2	0.300	6641.4	3.5
50	89.9	0.69	46.2	0.369	4156.9	5.3
25	50.3	0.41	46.4	0.208	2330.3	7.7
0	0.7	0.43	46.4	0.112	32.2	375.7

Table 17. Summary of ATC 13-kW Turboelectric performance at different throttle settings

Turbine Throttle (%)	Current (A)	Current Standard Dev. (A)	Voltage (V)	Voltage Standard Dev. (V)	Power (W)	BSFC lbm/(hp*hr)
100	236.1	2.24	41.7	0.252	9841	3.0
75	183.0	1.91	45.4	0.166	8306.1	3.7
50	96.5	0.92	44.9	1.1581	4329.8	5.3
25	16.3	0.47	43.8	0.282	715.0	18.1
0	1.7	3.16	44.6	0.189	74.1	93.6

Table 18 shows the maximum power to weight ratio of all three ATC turboelectric systems. Unlike in the DTC systems, the ATC 7-kW system has a lower PWR than the ATC 5-kW system.

However, the uncertainty of the ATC 7-kW system is larger than the difference in PWR between the ATC 5-kW and 7-kW systems, so the ATC 5-kW and 7-kW systems did not have a significant difference in PWR.

Table 18. Maximum power-to-weight ratio of each ATC turboelectric system.

System	PWR (hp/lbf)	PWR (kW/N)	Uncertainty ± (hp/lbf)
ATC 5-kW	0.39	0.065	0.005
ATC 7-kW	0.37	0.061	0.040
ATC 13-kW	0.52	0.087	0.006

Transient Performance

Identification of transient endpoints

A program was needed to be developed to determine where variations in voltage and current occurred. These variations were used to classify the transient regime of the throttle tests within the program. The first step involved cropping data around each throttle transient window so that the data only contained the transient and the steady-state period before and after the transient points. The data generally appeared, as shown in the example in Figure 26. Each test point had the turbine or load settled at one throttle point and was rapidly changed to another pre-determined point. The abrupt change noted can be seen in Figure 26, where the current is steady until it rapidly increases and settles at a new, higher steady point. Start and endpoints needed to be identified to extract the dynamic section from these data successfully. A running average of the last 20 points (n-20, n) was generated for every point in the data set to identify the starting point. The standard deviation of the previous 20 points was also calculated. An example of these averages can be seen in Figure 27. Once these values were calculated, the program would step through each point, n. The program would check if the next point, n + 1, exceeded 1 standard deviation from the running average.

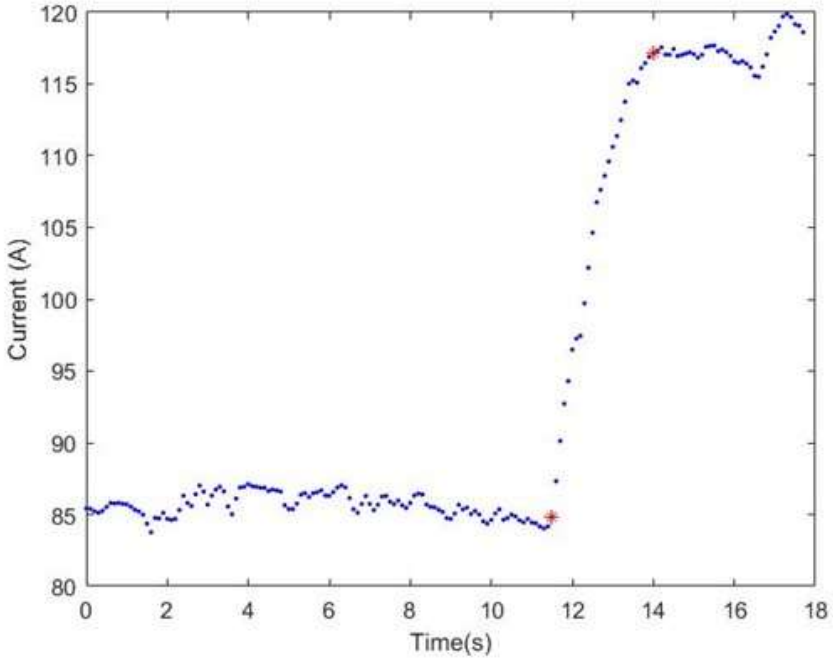

Figure 26. An example of transient throttle data displaying current as a function of time. The endpoints of the transient are marked in red.

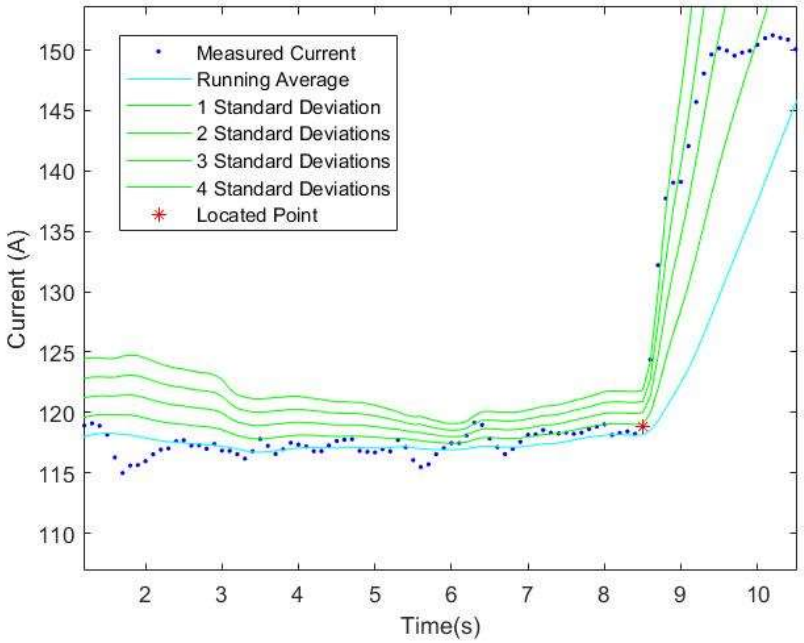

Figure 27. A plot showing measured currents, a running average, and positive multiples of the standard deviation

Similarly, if the n + 1 point exceeded ±1 standard deviation, the program would check if n + 2 exceeded ±2 standard deviations. This process was repeated for n + 3 and n + 4 against 3 and 4 standard deviations, respectively. If all four standard deviation comparisons were exceeded, then point n was considered the beginning point of the throttle transient. A similar process was used for the endpoint of the throttle transient. The endpoint program differed in that instead of using the last 20 points for the running average, the following 20 points (n, n + 20) were used. The program also ran from the end of the data set backward. This method was used instead of one which checks for consecutively rising points because there was a possibility that some data sets involved an extremely rapid change which occurred only over a few (<5) points. There was also the possibility of consecutively rising points not part of the transient test, as seen at approximately the 16-s mark in Figure 26. An algorithm based on the absolute magnitude of change at the beginning and end of the throttle transient could not be used because the magnitude of change varied between throttle tests (e.g., the 50–100% transient would have a more considerable shift in current than the 50–75%). The method used is advantageous as it automatically scales to the magnitude of change in current and avoids many potential false transient points.

DTC Performance

The program generated plots for throttle transients and compared them along shared axes using the algorithm described above. While current was used to determine the start and endpoints of the transient period, the power provided is a more pertinent parameter to compare different throttle steps. Figure 28 shows the change in power over time of the DTC 5-kW turboelectric system. For comparison, positive throttle step changes (e.g., a step change from 50% throttle to 75% throttle) were plotted together on one chart. The plot of each transient test was lined up in time based on their start point. The plots contain data from 2-s before the initiation of the transient up until the system reached a new steady point. This line-up process was performed on each of the transient test plots. The 50-75% and 50-100% tests started at a similar power output, corresponding to the

50% throttle. Similarly, the 75-100% and 50-100% tests ended at a similar power output. The 50-75% test had a slower response time than the other two test points. (4.6-s as opposed to roughly 1.5-s for the other two test points). Table 19 tabulates the response time at each test point, and the initial and final values of current, voltage, and power.

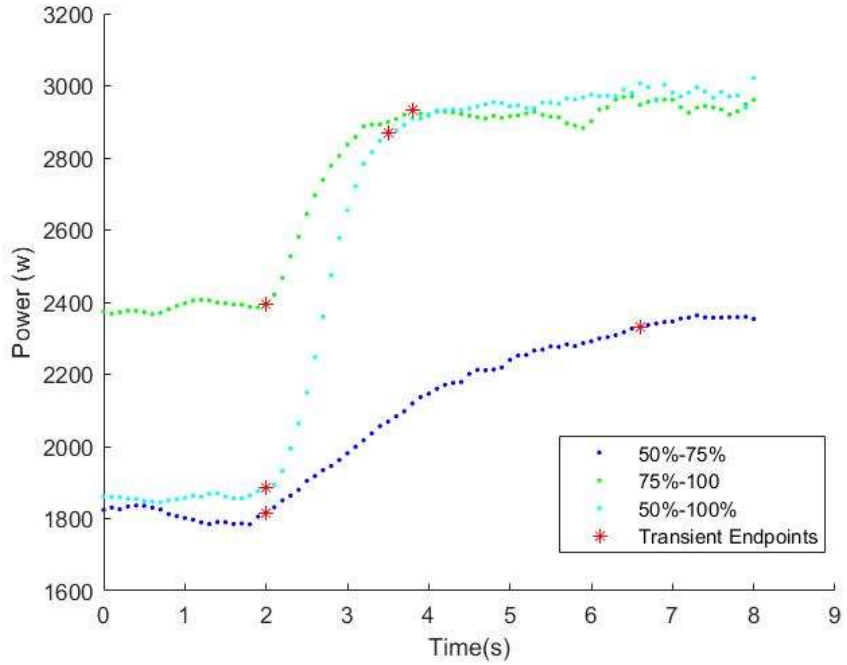

Figure 28. DTC 5-kW positive step changes in throttle position with endpoints marked

Table 19. DTC 5-kW positive step change in throttle position power data

Initial and Final Throttle (%)	Response Time (s)	Initial Current (A)	Final Current (A)	Initial Voltage (V)	Final Voltage (V)	Initial Power (W)	Final Power (W)
50% - 75%	4.5996	58.9	69.5	30.9	33.5	1817	2331
75% - 100%	1.7997	70.1	80.0	34.2	36.6	2396	2932
50% - 100%	1.5004	61.0	79.5	30.9	36.1	1886	2870

Similar tests were performed for negative steps in throttle settings for the turbine engine. Plots of power delivered over time by the DTC 5-kW system can be seen in Figure 29. Like the positive step change plots, the 100-50% and 100-75% tests started at a similar power output and the 100-50% and 75-50% finished at similar power outputs. Again, one of these tests resulted in a longer

response time than the other two. Table 20 shows the response data and delivered power information like the previous table. The negative step changes for the DTC 5-kW system took slightly longer than that of the positive step changes, with the shorter two taking roughly 2.5-s to reach their final power output, and the longer of the three taking 5.7-s to reach the final power output.

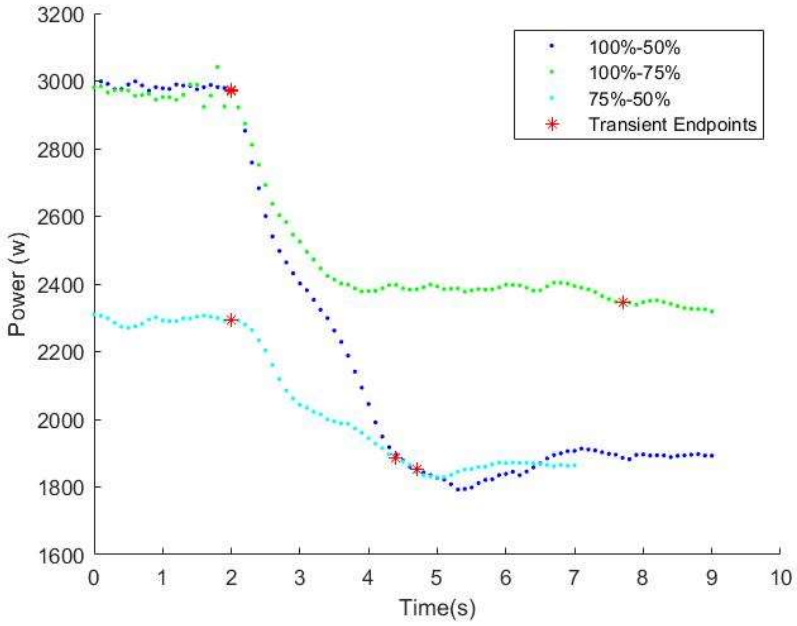

Figure 29. DTC 5-kW negative step changes in throttle position

Table 20. DTC 5-kW negative step change in throttle position power data

Initial and Final Throttle (%)	Response Time (s)	Initial Current (A)	Final Current (A)	Initial Voltage (V)	Final Voltage (V)	Initial Power (W)	Final Power (W)
100% - 50%	2.6997	82.0	60.6	36.2	30.6	2971	1852
100% - 75%	5.7005	81.2	69.6	36.6	33.7	2973	2345
75% - 50%	2.4003	68.8	60.9	33.3	31.0	2293	1886

Figure 30 shows the power delivered by the DTC 7-kW turboelectric system during the positive throttle step change tests. Initial observations show that the 50–100% test took nearly as long as the 50–75% test point to complete. The 50–100% test did not reach maximum power as soon as

the 75–100% test. The 50-75% and 50-100% tests started at a similar power output, though the 50-100% test did not reach as high of a power output as the 75-100% tests. Table 21 shows the response time and power data from the DTC 7-kW positive step change tests. Note that the longest response time was 2.5-s compared to the maximum of 5.7-s during the DTC 5-kW tests.

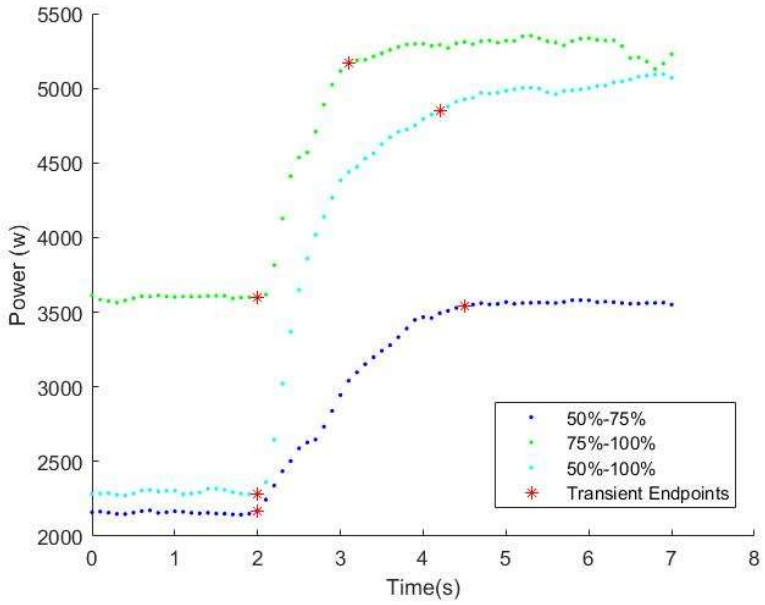

Figure 30. DTC 7-kW positive step changes in throttle position

Table 21. DTC 7-kW positive step change in throttle position power data

Initial and Final Throttle (%)	Response Time (s)	Initial Current (A)	Final Current (A)	Initial Voltage (V)	Final Voltage (V)	Initial Power (W)	Final Power (W)
50% - 75%	2.4997	84.8093	117.1548	25.587	30.2336	2170	3542
75% - 100%	1.1003	118.2284	150.1563	30.4068	34.3957	3595	5165
50% - 100%	2.2005	88.363	143.5384	25.8575	33.7751	2285	4848

Figure 31 shows the power delivered by the DTC 7-kW system during the negative throttle step tests. Like the DTC 5-kW negative step tests, the 100-50% and 100-75% tests started at a similar power output and the 100-50% and 75-50% finished at similar power outputs. A small dip can be seen in the 75-50% test, resulting this test taking longer to reach steady operation than it would have otherwise. The cause of this dip is not known. Table 22 shows the response time and power

data for these tests. The slowest response time was the 75-50% test, taking 3.2-s. This was slower than the slowest response time in the positive step tests.

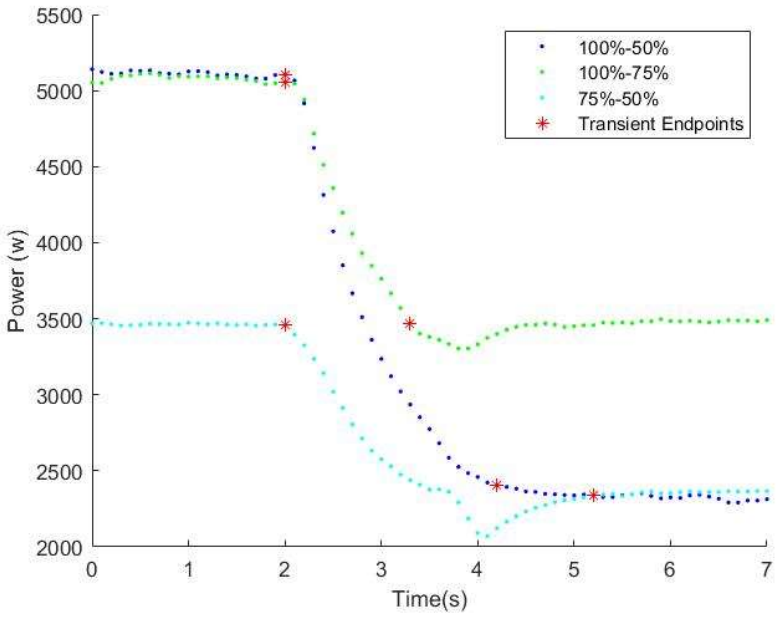

Figure 31. DTC 7-kW negative step changes in throttle position

Table 22. DTC 7-kW negative step change in throttle position power data

Initial and Final Throttle (%)	Response Time (s)	Initial Current (A)	Final Current (A)	Initial Voltage (V)	Final Voltage (V)	Initial Power (W)	Final Power (W)
100% - 50%	2.2006	147.0529	91.2085	34.7197	26.3614	5106	2404
100% - 75%	1.2998	147.6012	114.6095	34.252	30.28	5055.6	3470.5
75% - 50%	3.1999	116.227	90.7615	29.7343	25.7597	3455.9	2338

Figure 32 shows the power delivered by the DTC 13-kW system during the positive step tests. The positive step tests on the DTC 13-kW system qualitatively look smoother than the other tests, with no noteworthy dips or spikes in power. The 50-75% test took noticeably longer than the other two tests. Table 23 shows the response time and power data for these tests. The response time of the 75-100% and 50-100% were shorter than most of the other DTC tests, at about 1-second each.

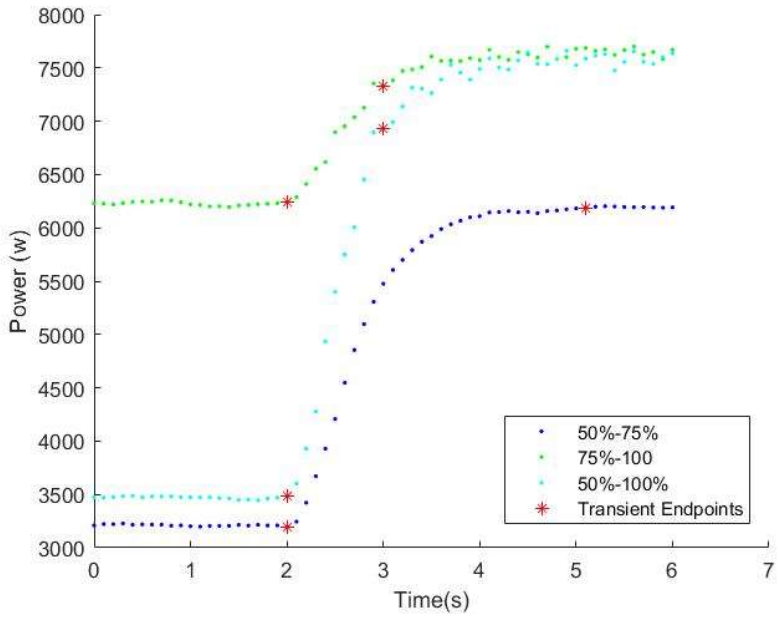

Figure 32. DTC 13-kW positive step changes in throttle position

Table 23. DTC 13-kW positive step change in throttle position power data

Initial and Final Throttle (%)	Response Time (s)	Initial Current (A)	Final Current (A)	Initial Voltage (V)	Final Voltage (V)	Initial Power (W)	Final Power (W)
50% - 75%	3.0994	117.7	179.8	27.2	34.4	3197	6189
75% - 100%	0.9997	180.0	200.6	34.7	36.6	6242	7333
50% - 100%	1.0007	124.4	196.3	28.0	35.3	3481	6936

Figure 33 shows the power delivered vs. time for the DTC 13-kW system during the negative throttle step tests. unlike most other tests, there is a significant difference between the final power in the 100-50% and 75% tests. In addition to this, the 75-50% test had a much slower response time than the other tests. Something else of note in this figure is that only 1 second of previous data can be shown before the beginning of the transients because of how the data was cropped during processing. Table 24 shows the response time and power data for these tests. The response time was in general longer for the negative steps than for the positive steps of the 13-kW system.

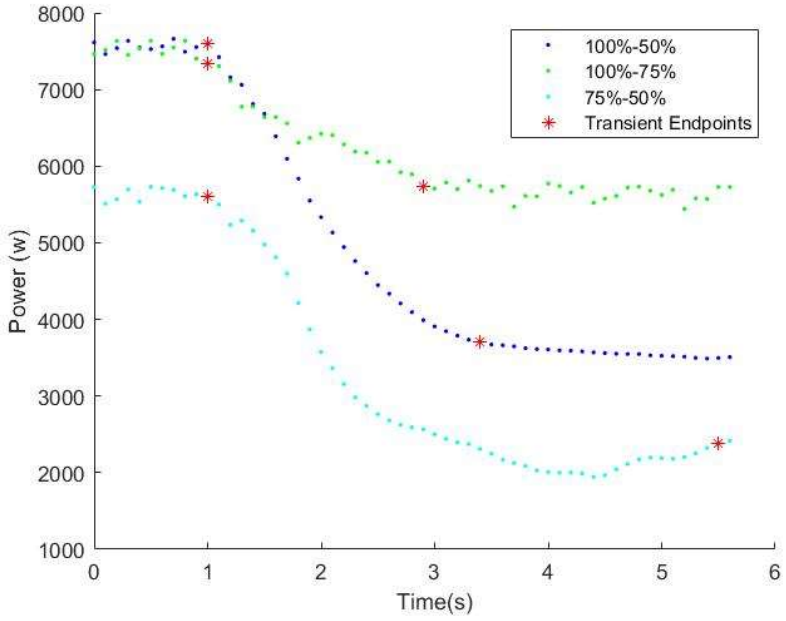

Figure 33. DTC 13-kW negative step changes in throttle position

Table 24. DTC 13-kW negative step change in throttle position power data

Initial and Final Throttle (%)	Response Time (s)	Initial Current (A)	Final Current (A)	Initial Voltage (V)	Final Voltage (V)	Initial Power (W)	Final Power (W)
100% - 50%	2.3995	204.4	128.9	37.2	28.8	7594	3707
100% - 75%	1.9	199.2	169.2	36.8	33.9	7337	5736
75% - 50%	4.4997	168.0	99.5	33.3	23.9	5600	2379

DTC Performance Discussion

The performance parameters compared between the three DTC turboelectric systems is the response time and the average slope of the power curve during the transient. Table 25 and Table 26 show the response time and average power slope for the DTC transient tests. There is a general lack of consistency in the results seen in the DTC tests. For example, the 5-kW system had a longer response time between 50% and 75% than between 50% and 100%. No singular cause could be identified for the lack of consistency in DTC response time results. Differences in response time could be caused by differences in the initial angular momentum of the system.

Differences in response time could also be caused by the different starting voltage and current across the test points. The difference in response time could also be caused by the programming of the ECU, which can vary the rate at which the turbine's throttle changes. There are too many variables that can affect the response time of the system that were not accounted for in the DTC tests. Therefore, no conclusive results can be drawn directly from the DTC transient tests.

Table 25. DTC Positive-step response time and average slope results

Test	50%-75%		75%-100%		50%-100%	
	Response Time (s)	Average Power Slope (W/s)	Response Time (s)	Average Power Slope (W/s)	Response Time (s)	Average Power Slope (W/s)
DTC 5-kW	4.6	112	1.8	298	1.5	656
DTC 7-kW	2.5	549	1.1	1427	2.2	1165
DTC 13-kW	3.1	965	1.0	1091	1.0	3453

Table 26. DTC Negative-step response time and average slope results

Test	100%-50%		100%-75%		75%-50%	
	Response Time (s)	Average Power Slope (W/s)	Response Time (s)	Average Power Slope (W/s)	Response Time (s)	Average Power Slope (W/s)
DTC 5-kW	2.7	-415	5.7	-110	2.4	-170
DTC 7-kW	2.2	-1227	1.3	-1219	3.2	-349
DTC 13-kW	2.4	-1620	1.9	-843	4.5	-716

ATC Performance

Transient tests were performed with the turbines controlled in the ATC configuration. In general, the ATC systems are capable of outputting more power than the DTC systems This increased power usage is because the available battery power can be supplied in conjunction with the power produced by the turbine, which differs from DTC, where the turbogenerator supplies the only power available. The batteries used were capable of approximately 2 kW of power output. As expected, the turboelectric system's maximum power output is approximately 2 kW higher in the

DTC mode than in the ATC mode of operation. Figure 34 shows the power delivered by the ATC 5-kW system during the positive-step transient tests. In general, the ATC tests of the 5-kW system had a much faster response time than the DTC 5-kW system. This is because the battery can provide almost instantaneous power (response time on the order of milliseconds) while the turbine takes longer time to respond (response time on the order of seconds). Like DTC tests, the initial and final power output at 50%, 75%, and 100% throttle appear to agree. Table 27 shows the response time and power data for these tests. Note that all three response times were under 1 second, with the shortest being 0.2-s. During the DTC tests, the shortest response time was 1.5-s.

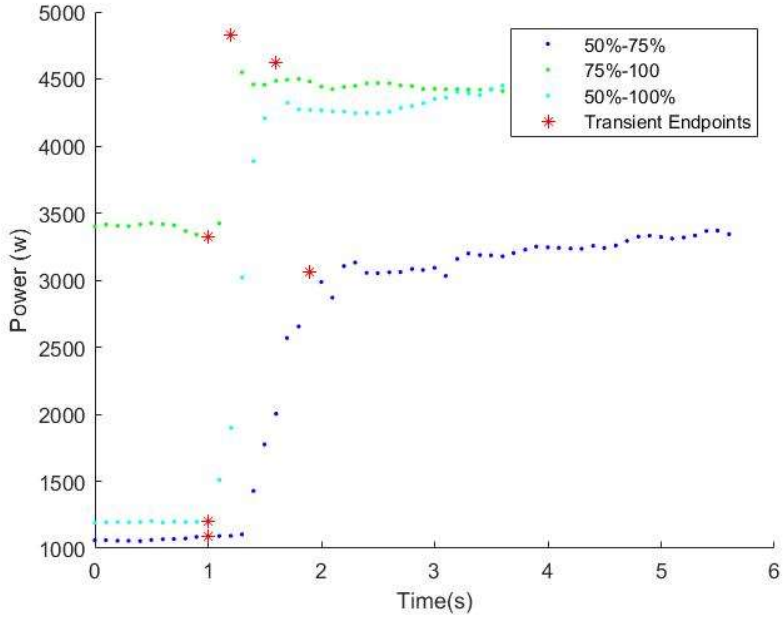

Figure 34. ATC 5-kW positive step changes in throttle position

Table 27. ATC 5-kW positive step change in throttle position power data

Initial and Final Throttle (%)	Response Time (s)	Initial Current (A)	Final Current (A)	Initial Voltage (V)	Final Voltage (V)	Initial Power (W)	Final Power (W)
50% - 75%	0.8983	23.6	71.3	46.2	42.9	1090	3059
75% - 100%	0.2	75.8	114.5	43.8	42.2	3319	4829
50% - 100%	0.6006	25.0	112.0	48.0	41.2	1201	4617

The negative-step transient tests were performed on the ATC 5-kW system. The result of these tests is shown in Figure 35. The 75-50% test had a slower response time than the other 2 tests. The response time is tabulated in Table 28. As expected, the 75-50% test had the slowest response time at 1.2-s, still shorter than the quickest response time during the 5-kW DTC tests at 1.5-s.

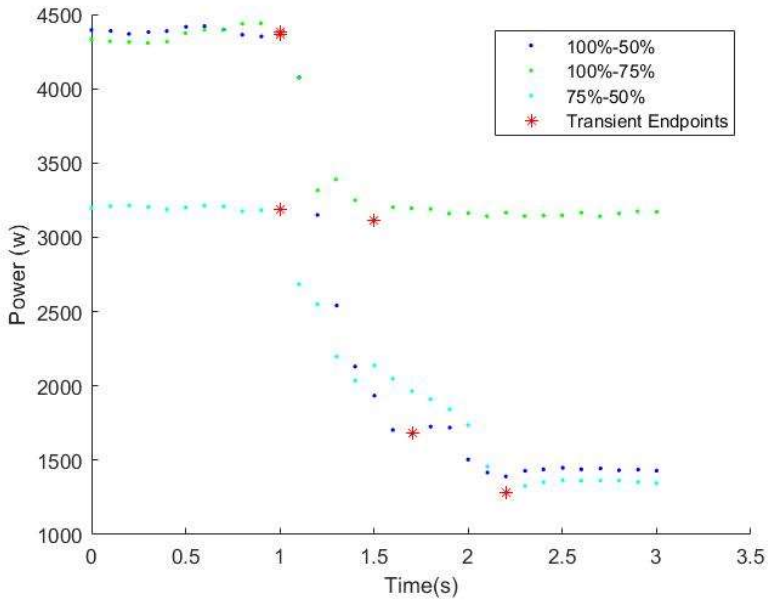

Figure 35. ATC 5-kW negative step changes in throttle position

Table 28. ATC 5-kW negative step change in throttle position power data

Initial and Final Throttle (%)	Response Time (s)	Initial Current (A)	Final Current (A)	Initial Voltage (V)	Final Voltage (V)	Initial Power (W)	Final Power (W)
100% - 50%	0.7025	103.5	33.5	42.2	50.1	4367	1679
100% - 75%	0.4986	104.5	71.5	41.9	43.5	4379	3113
75% - 50%	1.2003	73.2	24.7	43.6	51.9	3190	1281

Figure 36 shows the response of the ATC 7-kW system during the positive-step transient tests. Like the ATC 5-kW tests, the 50-100% and 75-100% tests had an extremely quick response time. The 50-75% test showed unusual behavior compared to the other two tests. An oscillation can be seen where the power reached a peak, then dipped back down before reaching its final power output. This oscillation is likely due to the controller not being optimally tuned. Under large throttle changes, some oscillatory behavior could occasionally be seen. Table 29 shows the response time and power data from these tests. As expected, the 50-75% test had the slowest response time (2.2-s). While this is slower than the fastest response time of the DTC 7-kW tests (1.2-s) it is still faster than the slowest response time (3.2-s). The 50-100% and 75-100% had faster response times than any of the DTC tests.

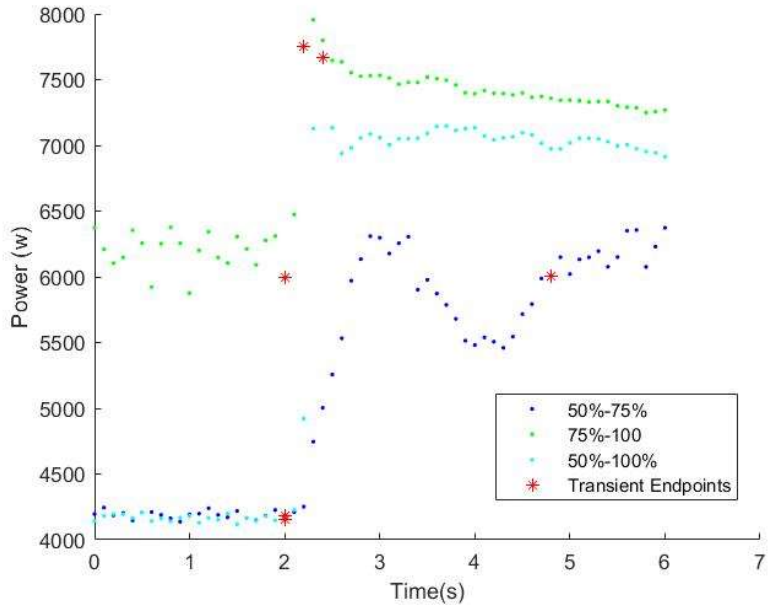

Figure 36. ATC 7-kW positive step changes in throttle position

Table 29. ATC 7-kW positive step change in throttle position power data

Initial and Final Throttle (%)	Response Time (s)	Initial Current (A)	Final Current (A)	Initial Voltage (V)	Final Voltage (V)	Initial Power (W)	Final Power (W)
50% - 75%	2.2	80.4	202.2	49.9	39.5	4013	7982
75% - 100%	0.1009	198.7	206.7	38.3	38.0	7600	7851
50% - 100%	0.3997	83.7	182.9	42.4	38.1	3545	6978

Figure 37 shows the power data from the ATC 7-kW negative-step transient tests. the 100-75% test does not appear to show a meaningful change in power compared to other tests. The other two test points showed changes in power at scales closer to what would be expected. The rcause of the small difference in power for the 100-75% test is believed to be because the power output at higher throttle levels is driven primarily by the battery, and the capability of the load to use power far outstrips the ability of the turboelectric system to deliver power. The turbine and battery are outputting near-maximum power, so even when the throttle on the load is reduced, the turboelectric system can deliver almost its entire power availability. Table 30 shows the response time and power data from these tests. Because of the small change in power output, the 100-75%

test had a quick response time (.3-s). The other two tests were slower than the positive-step tests, but still generally faster than the DTC tests.

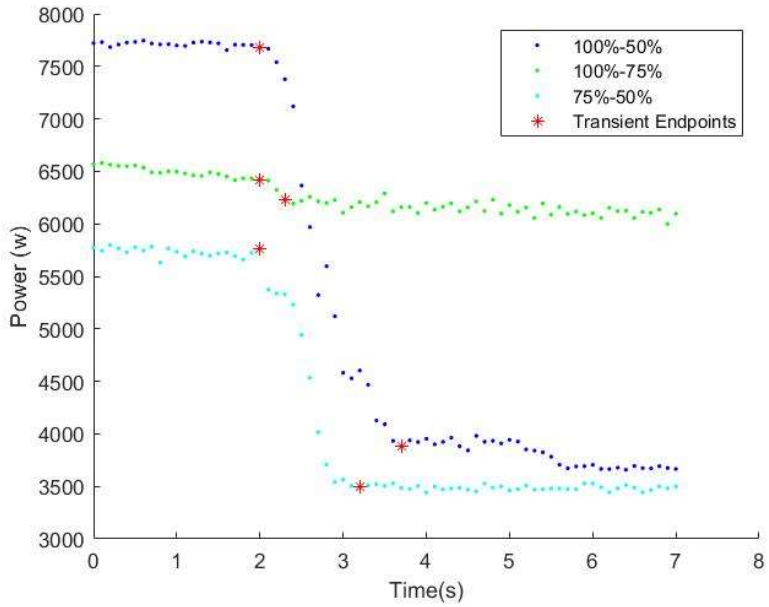

Figure 37. ATC 7-kW negative step changes in throttle position

Table 30. ATC 7-kW negative step change in throttle position power data

Initial and Final Throttle (%)	Response Time (s)	Initial Current (A)	Final Current (A)	Initial Voltage (V)	Final Voltage (V)	Initial Power (W)	Final Power (W)
100% - 50%	1.7009	202.2	81.3	38.0	47.7	7679	3880
100% - 75%	0.2991	171.8	165.8	37.4	37.6	6421	6231
75% - 50%	1.1997	154.9	85.9	37.2	40.6	5767	3492

Figure 38 shows the power output from the ATC 13-kW positive-step transient tests. One notable anomaly in the data from these tests is that the starting power in the 75-100% test and the finishing power in the 50-75% tests are different by almost 2-kW despite the intention that both points be at 75% throttle on the load. There is also around a 1-kW difference between the 50% throttle in the 50-75% test and the 50-100% test. The reason for these differences is not known. Table 31 shows the response time and power data from these tests. The 50-100% test had the slowest response time but was still shorter than most DTC response times.

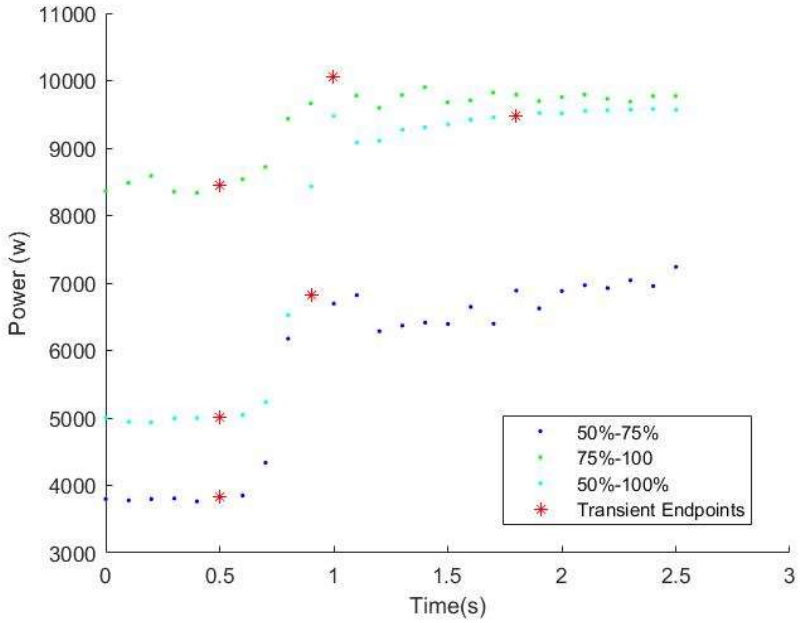

Figure 38. ATC 13-kW positive step changes in throttle position

Table 31. ATC 13-kW positive step change in throttle position power data

Initial and Final Throttle (%)	Response Time (s)	Initial Current (A)	Final Current (A)	Initial Voltage (V)	Final Voltage (V)	Initial Power (W)	Final Power (W)
50% - 75%	0.3999	83.4	163.5	45.9	41.7	3828	6821
75% - 100%	0.5007	185.0	241.6	45.6	41.6	8443	10055
50% - 100%	1.2982	112.7	232.3	44.4	40.8	5008	9472

Figure 39 shows the power delivered by the ATC 13-kW system during the negative-step transient tests. like the positive-step transient tests, the power delivered at 75% throttle is not consistent between the 100-75% and 75-50% tests. The same issue is seen with the 50% throttle during the 100-50% and 75-50% tests. The data is otherwise like the other ATC tests. Table 32 shows the response time and power data from these tests. All 3 tests were quick compared to both the ATC 13-kW positive step-transients and all 13-kW DTC transients.

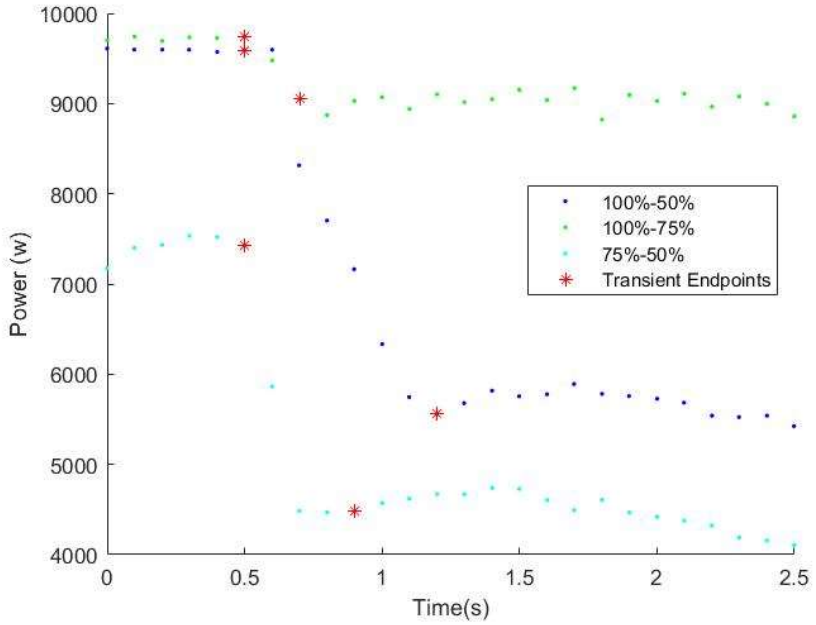

Figure 39. ATC 13-kW negative step changes in throttle position

Table 32. ATC 13-kW negative step change in throttle position power data

Initial and Final Throttle (%)	Response Time (s)	Initial Current (A)	Final Current (A)	Initial Voltage (V)	Final Voltage (V)	Initial Power (W)	Final Power (W)
100% - 50%	0.7016	233.1	107.3	41.2	51.8	9593	5559
100% - 75%	0.2	234.9	212.7	41.5	42.5	9746	9049
75% - 50%	0.3999	167.2	84.1	44.4	53.3	7425	4479

ATC Performance Discussion

Before discussing the results, it is essential to discuss the uncertainty in the measurements taken. The temporal resolution of the Pixhawk datalogger is 0.1 s, which means that there is a base level uncertainty of 0.05 s for each data point. Consider the response times shown above. For almost all data the ATC scheme responded far quicker than the DTC model. The difference in response time between ATC and DTC was significant compared to the temporal uncertainty of the Pixhawk. The results seen are not merely an artifact of instrument noise because the difference ATC and DTC response times lie far outside the 0.05 s uncertainty in timing.

Like the DTC results, there is no obvious trend in the response time of the three ATC systems. As discussed by Burgess et al. the response time of the ATC systems is generally faster than that of the DTC systems because the response time is primarily driven by the battery [44]. Unlike the DTC tests, however, no trend can be seen in the average power slope of the turboelectric systems. Like the response time data, there is no apparent order to which system had the highest and lowest on any given test. This result is expected as the response of the ATC systems is primarily driven by the battery and all three ATC systems used the same battery setup.

Table 33. ATC positive-step response time and average slope results

Test	50%-75%		75%-100%		50%-100%	
	Response Time (s)	Average Power Slope (W/s)	Response Time (s)	Average Power Slope (W/s)	Response Time (s)	Average Power Slope (W/s)
ATC 5-kW	0.9	2192	0.2	7548	0.6	5688
ATC 7-kW	2.2	1804	1.0	2490	0.4	8589
ATC 13-kW	0.4	7486	0.4	3219	1.3	3438

Table 34. ATC negative-step response time and average slope results

Test	100%-50%		100%-75%		75%-50%	
	Response Time (s)	Average Power Slope (W/s)	Response Time (s)	Average Power Slope (W/s)	Response Time (s)	Average Power Slope (W/s)
ATC 5-kW	0.7	-3827	0.5	-2538	1.2	-1590
ATC 7-kW	1.7	-2233	0.3	-637	1.2	-1896
ATC 13-kW	0.7	-5750	0.2	-3486	0.4	-7365

Electrical Safety

All three systems were designed to generate voltage around the 12-S range (39.6-V – 50.4-V). Theory would suggest that at a constant voltage, for the delivered power to increase, the current must also increase. If the current capacity of an electrical device is surpassed, the component can

fail. Higher currents also result in higher energy loss through heat. Electrical components must dissipate this additional thermal load, or the components will overheat and fail. Failures were especially seen in the switching circuitry of the battery augmentation system. Failures were primarily seen during discharge tests. The same battery system was used for all three turboelectric systems, so these failures do not provide much insight to the impact of turboelectric system scale on safety. Table 35 shows the maximum current delivered during the steady state tests. As expected, the current delivered increased as the power output of the turboelectric system increases. For both ATC and DTC, the maximum current of the 13-kW system is over twice the maximum current of the 5-kW system. As discussed in the theory section, the thermal load on components is proportional to the current squared. So while the current demand on the 13-kW system is over twice that of the 5-kW system, the required heat dissipation for the DTC 13-kW system is 6.7x higher than the DTC 5-kW and the required heat dissipation for the ATC 13-kW system is 4.6x higher than the ATC 5-kW system. This result was seen qualitatively as there were solder joints and components that failed during tests on the 13-kW system which did not fail on earlier tests on the 5-kW and 7-kW systems. As the scale of system increases, the current rating of devices must increase, while the heat dissipation requirement scales quadratically.

Table 35. Maximum current during the steady state tests

System	Maximum Current (A)
DTC 5-kW	81.7
DTC 7-kW	144.2
DTC 13-kW	211.2
ATC 5-kW	108.9
ATC 7-kW	170.2
ATC 13-kW	236.1

During transient tests, there is a risk that the generator could produce voltages high enough to damage electrical components, especially during the ATC tests where the turbine reacts to the

electrical load. In the ATC mode when the demanded power is decreased, the turbine engine will take some time to react, and some time to reach a lower RPM. During this time between the decreased load and lower turbine engine throttle setting, the generator speed can increase. The lower power demand reduces the current provided by the generator, and consequently reduces the torque applied to the turboprop, increasing shaft RPM. This increased RPM is paired with fewer losses within the generator itself to produce a voltage spike. The plots of voltage vs time for the three turboelectric systems can be seen in Figure 40 through Figure 42. The ATC 7-kW and 13-kW systems both reached a peak voltage before the voltage began to drop back down, while the ATC 5-kW system appeared to reach a peak voltage and stay the same. It is noteworthy that the peak voltage came after the marked end of the transients. This is because the endpoints of the transient tests were defined by the current curve of the system, and not the voltage. This shows that it is possible for the current output of the system can reach steady operation without the voltage reaching steady state.

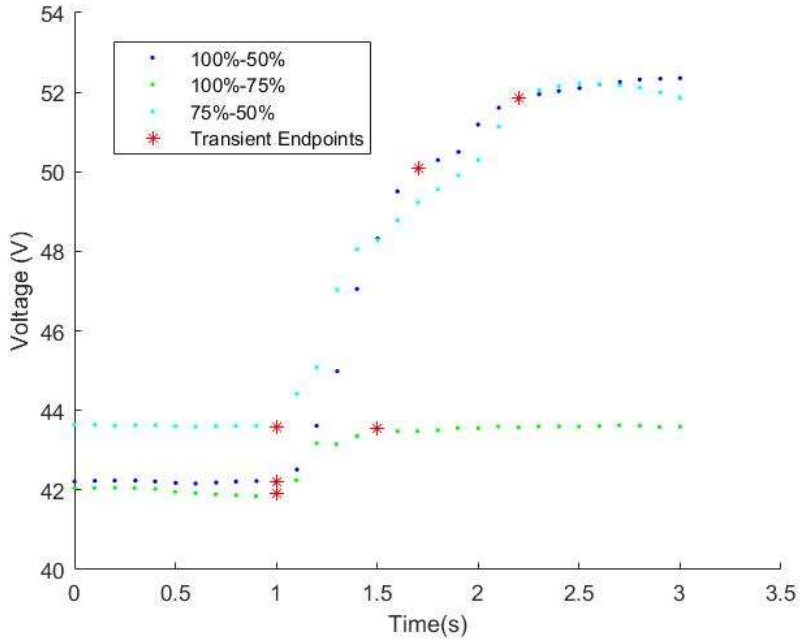

Figure 40. A plot of voltage over time for the ATC 5-kW negative step transient tests

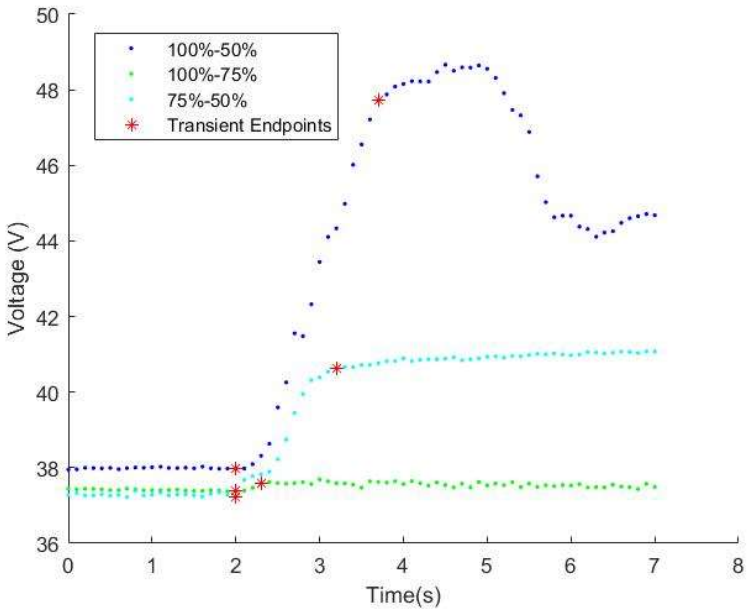

Figure 41. A plot of voltage over time for the ATC 7-kW negative step transient tests

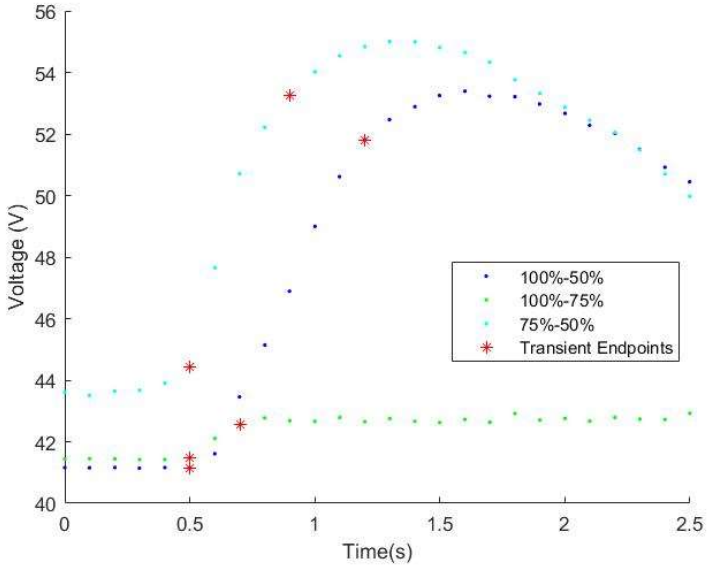

Figure 42. A plot of voltage over time for the ATC 13-kW negative step transient tests

The voltage spike seen in ATC tests was not seen during the DTC tests because the response of the DTC systems is driven by the turboprop itself. There is no 'lag' in the system like in ATC tests. The throttle signal goes directly to the turboprop engine. The opposite trend is seen where

the voltage decreases during the negative step transient tests. This is because the lower throttle sent to the turbine engine reduces the generator RPM.

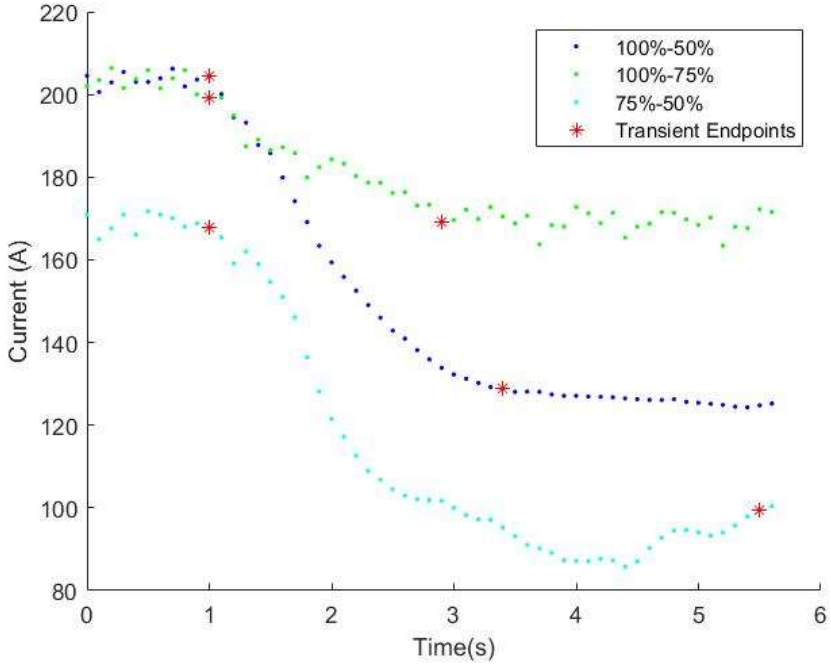

Figure 43. A plot of voltage over time for the DTC 13-kW negative step transient tests

Table 36 shows the peak voltage during the 100%-50% transient tests. no definitive trend can be seen in the peak voltage of the ATC systems. It is possible that the lower peak voltage seen by the ATC 7-kW system is due to better turboprop – generator compatibility. This is also thought to be why the DTC 7-kW system had the best electrical efficiency (compared to the rated power output of the engine) in steady state tests. It is thought that at 100% throttle, the 7-kW system is operating the closest to the turboprop's peak RPM, while the excess torque of the generators on the 5-kW and 13-kW systems causes the RPM to decrease. When this load is removed, the 5-kW and 13-kW systems can spin to a higher RPM because they were at a lower initial RPM before the transient. The dynamics of this interaction are complicated and would require further studies to reduce the impact of this voltage spike.

Table 36. Ending voltage of 100%-50% transient tests

System	Peak Voltage (V)
ATC 5-kW	52
ATC 7-kW	49
ATC 13-kW	55

CHAPTER V

Summary and Conclusions

This paper presents the experimental results of three different UAS scale turboelectric systems in a ground test configuration. The results of this paper are a key steppingstone in understanding the performance of turboelectric systems, which enables further work to prepare turboelectric systems for flight operations. Performance data from these turboelectric systems can be used in the future for further studies such as mission analysis. The results from this study will allow future aircraft designers to make informed decisions for the powerplant of hybrid-electric unmanned aircraft.

Steady State

As expected, in DTC tests, the most powerful K-100TP-based system output the most rectified power, and the K-45TP-based system had the lowest rectified power output. The reverse trend was seen in the BSFC of the systems, likely due to increased compressor pressure ratio and consequently increased thermal efficiency of the larger systems. The effect of increasing thermal efficiency with increasing scale dominates over the effect of decreasing electrical efficiency with increasing scale. This trend of increased power and decreased BSFC would be seen with larger turboelectric systems; however, this paper shows that there is a potential of diminishing improvement. There was also a notable power-to-weight improvement from the smaller K-45TP to larger K-100TP systems, though an improved, lightweight housing for the K-60TP system would likely resolve the trend better. With further optimization, the K-60TP system could potentially realize a power to weight ratio of 0.098-kW/N (0.58-hp/lbf), approaching the

PWR of the K-100TP system. Further optimization of the generator k_v could also see better power extraction from the K-100TP and K-45TP system.

It can be concluded that at the UAV scale, turboelectric power systems become more efficient as scale increases. It is possible that optimizations could be made to reduce weight and improve electrical system efficiency of the DTC systems, including active rectification and better electrical system component matching in terms of rated power, voltage, current, and k_v specifications.

ATC steady state tests showed that a battery could be run in parallel with the turboelectric system The battery allows the system to maintain a higher voltage during the tests and allows the systems to achieve a higher power output. Steady state tests also showed that results of the ATC system are impacted by the performance of the turbogenerator, the configuration of the controller, and the state of charge of the battery.

Transient

The data for the DTC transient tests was not conclusive enough to draw any conclusions as to the impact of scale on dynamic response of the system. Future works would be needed to better study the dynamic response of the DTC system. As expected, there was no trend seen in the ATC tests. The response of the ATC systems was primarily driven by the battery, evidenced by the faster response when times compared to the DTC systems. The same battery system was used between all three ATC systems, so it would be expected that the scale of the turbogenerator would not have a significant impact on the response of the turboelectric system.

A key area of interest for hybrid power systems in aircraft is in VTOL and multi-rotor applications. It is in these areas where the quicker response time seen in the ATC mode is vital. It is also essential that the pilot is not directly responsible for controlling the turbine power output magnitude for VTOL and multi-rotor flight. Each of the VTOL rotors operates at different power levels to maintain steady and level flight, which is a power source that can react to the changing

demands in real-time. The pilot controls the other four primary controls (roll, pitch, yaw, and throttle). Adding a fifth control input, which must be carefully balanced, would overburden the pilot during flight. From the pilot perspective, ATC is generally preferred in all flight cases.

There are situations, however, where DTC would be advantageous. An example of when DTC could be utilized is using a conventional, fixed-wing aircraft. The pilot could directly control the turbine and allow the electric propulsors to respond accordingly based on the power made available by the turbogenerator at any given time. Using DTC can save weight compared to ATC configurations by not having switching circuitry or additional power batteries. Fixed-wing aircraft have a much more responsive throttle with the ATC control scheme than the DTC.

The more responsive ATC scheme is generally preferable to the pilot. In other words, the ATC control scheme more accurately imitates battery power output, whereas the DTC scheme behaves more like a turbine. ATC offers additional advantages to safety. The active control scheme has the potential to provide better instrumentation and state determination for the turboelectric system. This instrumentation can govern the turboelectric system and ensure it is behaving correctly and not risking damage to the rest of the power system. Having a battery in the loop for a VTOL system can also add redundancy by ensuring a VTOL aircraft can land even if the turbine fails in flight.

Electrical Safety

As discussed in the results section, the current seen during steady state tests more than doubled between the largest and smallest systems. This is because, if system voltage is kept constant, current increases linearly with power. However, the thermal dissipation requirement increases quadratically with increasing current. Therefore, if system voltage is held constant, the thermal loading of electrical components will increase quadratically. It could potentially be advantageous to increase the voltage of the system for larger turboelectric systems to reduce the necessary current ratings for electrical components and reduce the thermal dissipation demands for the

electrical components. Increased voltage has the added benefit of potentially increasing the electrical efficiency of the system by reducing the ohmic loses within the system. However, increased voltage comes with additional challenges with battery integration for the turboelectric system. To achieve a higher voltage with a battery pack, more battery cells must be placed in series. The more cells used in a battery system, the more hardware is required to balance and protect the extra battery cells. Future works could investigate the impact of changing voltage on the weight and performance of these turboelectric systems.

Conclusion

The impact of this paper is another key steppingstone in understanding the performance of turboelectric systems, which enables future work to develop such turboelectric systems and integrate them with aircraft for flight operations. Observations from this paper assist UAS designers to make informed decisions about trade-offs in terms of power, weight, and volume, including an appropriate combination of power from combustion engines and batteries. The usage of COTS parts in this study has allowed for faster prototyping and analysis of turboelectric systems; however, there is much more work to be done to further optimize these systems to reduce weight and increase power output for flight operations. Performance data from these turboelectric systems can be used in further studies such as airframe integration, mission analysis, operational planning to study feasibility of using turboelectric systems for unmanned aircraft, including flight tests at different speeds and altitudes. Additional future work can compare these turboelectric systems to other powerplants such as piston-hybrids and battery-only aircraft to assist designers with making decisions about the most appropriate system based on the type of mission and expected flight speeds and altitudes.

REFERENCES

[1] Harris Aerial, and Ambition Insight. CARRIER H6 HYBRID . *https://www.harrisaerial.com/carrier-h6-hybrid-drone/*.

[2] Wilkerson, J. T., Jacobson, M. Z., Malwitz, A., Balasubramanian, S., Wayson, R., Fleming, G., Naiman, A. D., and Lele, S. K. "Analysis of Emission Data from Global Commercial Aviation: 2004 and 2006." *Atmospheric Chemistry and Physics*, Vol. 10, No. 13, 2010, pp. 6391–6408. https://doi.org/10.5194/acp-10-6391-2010.

[3] OWENS, R., HASEL, K., and MAPES, D. Ultra High Bypass Turbofan Technologies for the Twenty-First Century. 1990.

[4] Tobi, A. L. M., and Ismail, A. E. "Development in Geared Turbofan Aeroengine." *IOP Conference Series: Materials Science and Engineering*, Vol. 131, 2016, p. 012019. https://doi.org/10.1088/1757-899X/131/1/012019.

[5] Alexiou, A., Aretakis, N., Roumeliotis, I., Kolias, I., and Mathioudakis, K. Performance Modelling of an Ultra-High Bypass Ratio Geared Turbofan. 2017.

[6] Ralph Jansen. NASA Electrified Aircraft Propulsion (EAP). *https://www1.grc.nasa.gov/aeronautics/eap/*.

[7] Welstead, J., and Felder, J. L. Conceptual Design of a Single-Aisle Turboelectric Commercial Transport with Fuselage Boundary Layer Ingestion. 2016.

[8] Felder, J., Kim, H., and Brown, G. Turboelectric Distributed Propulsion Engine Cycle Analysis for Hybrid-Wing-Body Aircraft. 2009.

[9] Dae Kim, H., L. Felder, J., T. Tong, M., J. Berton, J., and J. Haller, W. "Turboelectric Distributed Propulsion Benefits on the N3-X Vehicle." *Aircraft Engineering and Aerospace Technology*, Vol. 86, No. 6, 2014, pp. 558–561. https://doi.org/10.1108/AEAT-04-2014-0037.

[10] Kim, H. D., Brown, G. v., and Felder, J. L. Distributed Turboelectric Propulsion for Hybrid Wing Body Aircraft. 2008.

[11] Schiltgen, B. T., and Freeman, J. ECO-150-300 Design and Performance: A Tube-and-Wing Distributed Electric Propulsion Airliner. 2019.

[12] Gibson, A., Hall, D., Waters, M., Masson, P., Schiltgen, B., Foster, T., and Keith, J. The Potential and Challenge of TurboElectric Propulsion for Subsonic Transport Aircraft. 2010.

[13] Pornet, C., Gologan, C., Vratny, P. C., Seitz, A., Schmitz, O., Isikveren, A. T., and Hornung, M. "Methodology for Sizing and Performance Assessment of Hybrid Energy Aircraft." *Journal of Aircraft*, Vol. 52, No. 1, 2015, pp. 341–352. https://doi.org/10.2514/1.C032716.

[14] Thipphavong, D. P., Apaza, R., Barmore, B., Battiste, V., Burian, B., Dao, Q., Feary, M., Go, S., Goodrich, K. H., Homola, J., Idris, H. R., Kopardekar, P. H., Lachter, J. B., Neogi, N. A., Ng, H. K., Oseguera-Lohr, R. M., Patterson, M. D., and Verma, S. A. Urban Air Mobility Airspace Integration Concepts and Considerations. 2018.

[15] Hendricks, E. S., Falck, R. D., Gray, J. S., Aretskin-Hariton, E., Ingraham, D., Chapman, J. W., Schnulo, S. L., Chin, J., Jasa, J. P., and Bergeson, J. D. Multidisciplinary Optimization of a Turboelectric Tiltwing Urban Air Mobility Aircraft. 2019.

[16] Cinar, G., Markov, A. A., Gladin, J. C., Garcia, E., Mavris, D. N., and Patnaik, S. S. Feasibility Assessments of a Hybrid Turboelectric Medium Altitude Long Endurance Unmanned Aerial Vehicle. 2020.

[17] Markov, A., Cinar, G., Gladin, J. C., Garcia, E., Denney, R. K., Patnaik, S. S., and Mavris, D. N. Performance Assessment of a Distributed Electric Propulsion System for a Medium Altitude Long Endurance Unmanned Aerial Vehicle. 2021.

[18] Harmats, M., and Weihs, D. "Hybrid-Propulsion High-Altitude Long-Endurance Remotely Piloted Vehicle." *Journal of Aircraft*, Vol. 36, No. 2, 1999, pp. 321–331. https://doi.org/10.2514/2.2443.

[19] Harmon, F. G., Frank, A. A., and Chattot, J.-J. "Conceptual Design and Simulation of a Small Hybrid-Electric Unmanned Aerial Vehicle." *Journal of Aircraft*, Vol. 43, No. 5, 2006, pp. 1490–1498. https://doi.org/10.2514/1.15816.

[20] Harmon, F. G., Frank, A. A., and Joshi, S. S. "The Control of a Parallel Hybrid-Electric Propulsion System for a Small Unmanned Aerial Vehicle Using a CMAC Neural Network." *Neural Networks*, Vol. 18, Nos. 5–6, 2005, pp. 772–780. https://doi.org/10.1016/j.neunet.2005.06.030.

[21] Harmon, F. G., Frank, A. A., Chattot, J.-J., and Joshi, S. S. *Neural Network Control of a Parallel Hybrid-Electric Propulsion System for a Small Unmanned Aerial Vehicle*. 2004.

[22] Frank, A. Charge Depletion Control Method and Apparatus for Hybrid Powered Vehicles, 5,842,534, 1998.

[23] Frank, A. Control Method and Apparatus for Internal Combustion Engine Electric Hybrid Vehicles, 6,054,844, 2000.

[24] Sergent, A., Ramunno, M., D'Arpino, M., Canova, M., and Perullo, C. Optimal Sizing and Control of Battery Energy Storage Systems for Hybrid Turboelectric Aircraft. 2020.

[25] Connolly, J. W., Chapman, J. W., Stalcup, E. J., Hunker, K. R., Chicatelli, A. K., and Thomas, G. L. Modeling and Control Design for a Turboelectric Single Aisle Aircraft Propulsion System. 2018.

[26] Seok, J., Kolmanovsky, I., and Girard, A. Integrated/Coordinated Control of Aircraft Gas Turbine Engine and Electrical Power System: Towards Large Electrical Load Handling. 2016.

[27] Zong, J., Zhu, B., Hou, Z., Yang, X., and Zhai, J. "Evaluation and Comparison of Hybrid Wing VTOL UAV with Four Different Electric Propulsion Systems." *Aerospace*, Vol. 8, No. 9, 2021, p. 256. https://doi.org/10.3390/aerospace8090256.

[28] Eqbal, M., Fernando, N., Marino, M., and Wild, G. "Development of a Turbo Electric Distribution System for Remotely Piloted Aircraft Systems." *Journal of Aerospace Technology and Management*, Vol. 13, 2021. https://doi.org/10.1590/jatm.v13.1209.

[29] Badum, L., Leizeronok, B., and Cukurel, B. "New Insights From Conceptual Design of an Additive Manufactured 300 W Microgas Turbine Toward Unmanned Aerial Vehicle Applications." *Journal of Engineering for Gas Turbines and Power*, Vol. 143, No. 2, 2021. https://doi.org/10.1115/1.4048695.

[30] Tanaka, S., Hikichi, K., Togo, S., Murayama, M., Hirose, Y., Sakurai, T., Yuasa, S., Teramoto, S., Niino, T., Mori, T., Esashi, M., and Isomura, K. "World's Smallest Gas Turbine Establishing Brayton Cycle." *7th International Workshop on Micro and Nanotechnology for Power Generation and Energy Conversion Applications (PowerMEMS 2007)*, 2007.

[31] Isomura, K., Murayama, M., and Kawakubo, T. Feasibility Study of a Gas Turbine at Micro Scale. 2001.

[32] Fréchette, L., Jacobson, S., Breuer, K., Ehrich, F., Ghodssi, R., and Zhang, X. "DEMONSTRATION OF A MICROFABRICATED HIGH-SPEED TURBINE SUPPORTED ON GAS BEARINGS." 2008.

[33] Epstein, A. H., Jacobson, S. A., Protz, J. M., and Frechette, L. G. SHIRTBUTTON-SIZED GAS TURBINES: THE ENGINEERING CHALLENGES OF MICRO HIGH SPEED ROTATING MACHINERY. 2000.

[34] Epstein, A. H. "Millimeter-Scale, Micro-Electro-Mechanical Systems Gas Turbine Engines." *Journal of Engineering for Gas Turbines and Power*, Vol. 126, No. 2, 2004, pp. 205–226. https://doi.org/10.1115/1.1739245.

[35] Han, S., Seo, J., Park, J., Choi, B.-S., and Do, K. H. DESIGN AND SIMULATION OF 500 W ULTRA-MICRO GAS TURBINE GENERATOR. 2010.

[36] Seo, J., Park, J. Y., Choi, B. S., and Park, M. R. "Performance Evaluation of Compressor to Develop 500W Class Ultra-Micro Gas Turbine." *Journal of Fluid Machinery*, Vol. 15, No. 6, 2012, pp. 51–57. https://doi.org/10.5293/kfma.2012.15.6.051.

[37] Seo, J. M., Park, J. Y., and Choi, B. S. "Start-up and Self-Sustain Test of 500 W Ultra-Micro Gas Turbine Generator." *Journal of Physics: Conference Series*, Vol. 476, 2013, p. 012060. https://doi.org/10.1088/1742-6596/476/1/012060.

[38] Seo, J., Lim, H.-S., Park, J., Park, M. R., and Choi, B. S. "Development and Experimental Investigation of a 500-W Class Ultra-Micro Gas Turbine Power Generator." *Energy*, Vol. 124, 2017, pp. 9–18. https://doi.org/10.1016/j.energy.2017.02.012.

[39] Rouser, K. P., Lucido, N., Durkee, M., Bellcock, A., and Zimbelman, T. Development of Turboelectric Propulsion and Power for Small Unmanned Aircraft. 2018.

[40] Moody, K. J., Replogle, C., and Rouser, K. P. Design, Characterization, and Integration of a Turboelectric Power System for Small Unmanned Multirotor Aircraft. 2019.

[41] Moody, K. J., Replogle, C. J., and Rouser, K. P. "Validation of Analytical Model for Turboelectric Power System for Preliminary Design Purposes." *Journal of Engineering for Gas Turbines and Power*, Vol. 142, No. 8, 2020. https://doi.org/10.1115/1.4046757.

[42] Moody, K. J. Active Throttle Control Model for a Small Unmanned Aircraft Turboelectric Power System. 2019.

[43] Runnels, T. R., Burgess, J. M., Johnsen, J. P., and Rouser, K. P. Experimental Study of 5-KW, 7-KW, and 13-KW Unmanned Aircraft Turboelectric Power Systems. 2021.

[44] Burgess, J., Runnels, T., Johnsen, J., Drake, J., and Rouser, K. "Experimental Comparison of Direct and Active Throttle Control of a 7 KW Turboelectric Power System for Unmanned Aircraft." *Applied Sciences*, Vol. 11, No. 22, 2021, p. 10608. https://doi.org/10.3390/app112210608.

[45] Jansen, R., Bowman, C., Jankovsky, A., Dyson, R., and Felder, J. Overview of NASA Electrified Aircraft Propulsion (EAP) Research for Large Subsonic Transports. 2017.

[46] Mattingly, J. D., and Boyer, K. M. *Elements of Propulsion: Gas Turbines and Rockets, Second Edition*. American Institute of Aeronautics and Astronautics, Inc., Washington, DC, 2016.

[47] Society of Automotive Engineers. *Gas Turbine Engine Performance Station Identification and Nomenclature Aerospace Reccomended Practice (ARP) 755A*. Warrendale, Pa, 1974.

[48] Gundlach, J. *Designing Unmanned Aircraft Systems*. American Institute of Aeronautics and Astronautics, Reston ,VA, 2012.

[49] Lithium-Ion Battery. https://www.cei.washington.edu/education/science-of-solar/battery-technology/.

APPENDICES

Parametric Cycle Analysis

Below is the Mathcad code used to perform the parametric cycle analysis described in the methodology section

$F_{ref} := 60N \qquad SFC_{ref} := \frac{.99}{hr} \qquad \pi_{cref} := 1.8 \quad T_{t4ref} := 2000R = 2000 \cdot R$

Technology Level 1

$\pi_{dmax} := .9 \quad e_c := .85 \quad \pi_b := .9 \quad \eta_b := .88 \quad e_t := .85 \quad \pi_{AB} := 1 \quad \eta_{AB} := 1$

$\pi_n := 1 \quad \eta_m := .95$

$cp_c := 0.24 \frac{BTU}{lbm \cdot R} \quad cp_t := 0.276 \frac{BTU}{lbm \cdot R} \quad \gamma_c := 1.4 \quad \gamma_t := 1.33 \quad g_c := 32.2 \frac{lbm \cdot ft}{lbf \cdot s^2}$

$P_{0ref} := 2116.2 \frac{lbf}{ft^2} \quad T_{0ref} := 518.69R \quad \rho_{0ref} := .07647 \frac{lbm}{ft^2} \quad M_{ref} := 0$

$h_{pr} := 18400 \frac{BTU}{lbm} \quad T_{t7max} := 2500R$

1.

$V_{0ref} := 0 \frac{ft}{s}$ Sea level Static Condition $\theta_{0ref} := 1$

$T_{t2ref} := T_{0ref} \cdot \left[1 + \frac{(\gamma_c - 1)}{2} \cdot M_{ref}^2\right]$ $T_{t2ref} = 518.69 \cdot R$

$T_{t4ref} = 2000 \cdot R$

$\pi_c := \pi_{cref}$ Static $\pi_{rref} := 1$

$\tau_{rref} := 1$

$\pi_{cref} = 1.8$

$\tau_{cref} := \pi_{cref}^{\frac{(\gamma_c - 1)}{\gamma_c \cdot e_c}}$ $\tau_{cref} = 1.218$

$$T_{t3ref} := T_{t2ref} \cdot \tau_{cref} = 631.995 \cdot R$$

$$h_{t3ref} := cp_c \cdot T_{t3ref} = 151.679 \cdot \frac{Btu}{lbm}$$

$$h_{t4ref} := cp_t \cdot T_{t4ref} = 552 \cdot \frac{Btu}{lbm}$$

$$f_{ref} := \frac{(h_{t4ref} - h_{t3ref})}{\eta_b \cdot h_{pr} - h_{t4ref}}$$

$f_{ref} = 0.026$

$$mdot_{4ref} := mdot_{0ref} \cdot (1 + f_{ref}) = 0.339 \frac{lb}{s}$$

$$mdot_0 \cdot cp_c (T_{T3} - T_{T2}) = \eta_m \cdot mdot_4 \cdot (T_{t4} - T_{t5})$$

$$T_{t45ref} := T_{t4ref} - \frac{1}{(1 + f_{ref}) \cdot \eta_m} \frac{cp_c}{cp_t} (T_{t3ref} - T_{t2ref})$$

$$\tau_{tHref} := \frac{T_{t45ref}}{T_{t4ref}} = 0.949$$

$\tau_{tHref} = 0.949$

$$\pi_{tHref} := \tau_{tHref}^{\frac{(\gamma_t)}{(\gamma_t - 1) \cdot e_t}}$$

$\pi_{tHref} = 0.782$

$$P_{T45} := P_{0ref} \cdot (\pi_{rref} \cdot \pi_{dmax} \cdot \pi_{cref} \cdot \pi_b \cdot \pi_{tHref}) = 16.754\,psi$$

LPT

Assume $P_{T9} := P_{0ref}$

$$\pi_{tLref} := \frac{P_{T9}}{P_{T45}} = 0.877$$

$$\tau_{tLref} := \pi_{tLref}^{\frac{[(\gamma_t - 1) \cdot e_t]}{\gamma_t}} = 0.973$$

$T_{T5ref} := T_{t45ref} \cdot \tau_{tLref} = 1847.112 \cdot R$

$mdot_{0ref} \equiv .15 \frac{kg}{s} = 0.331 \frac{lb}{s}$

$Wdot_{tL} := mdot_{4ref} \cdot cp_t \cdot \left(T_{t45ref} - T_{T5ref}\right) = 5112.354\,W$

$mdot_f := mdot_{0ref} \cdot f_{ref} = 0.008 \frac{lb}{s}$

$Wdot_E := .77 \cdot Wdot_{tL} = 3936.513\,W$

$Wdot_E = 5.279 \cdot hp$

$BSFC := \frac{mdot_f}{Wdot_E} = 5.772 \cdot \frac{lbm}{hp \cdot hr}$

VITA

Timothy Raymond Runnels

Candidate for the Degree of

Master of Science

Thesis: SCALING EFFECTS OF 5- TO 13-kW TURBOELECTRIC UNMANNED AIRCRAFT POWER SYSTEMS

Major Field: Mechanical and Aerospace Engineering

Biographical:

Education:

Completed the requirements for the Master of Science in Mechanical and Aerospace Engineering at Oklahoma State University, Stillwater, Oklahoma in May, 2022

Completed the requirements for the Bachelor of Science Mechanical and Aerospace Engineering at Oklahoma State University, Stillwater, Oklahoma in 2020.

Experience:

Research Intern, Autonomous Physics Group

Graduate Research Assistant, Stillwater Aerospace Propulsion and Power

Professional Memberships:

American Institute of Aeronautics and Astronautics
Sigma Gamma Tau Aerospace Engineering Honor Society